A PRIMER ON NOISE-INDUCED TRANSITIONS IN APPLIED DYNAMICAL SYSTEMS

ERIC FORGOSTON* AND RICHARD O. MOORE†

Abstract. Noise plays a fundamental role in a wide variety of physical and biological dynamical systems. It can arise from an external forcing or due to random dynamics internal to the system. It is well established that even weak noise can result in large behavioral changes such as transitions between or escapes from quasi-stable states. These transitions can correspond to critical events such as failures or extinctions that make them essential phenomena to understand and quantify, despite the fact that their occurrence is rare. This article will provide an overview of the theory underlying the dynamics of rare events for stochastic models along with some example applications.

Key words. Dynamical systems, escape, extinction, mean exit time, large deviation theory, mode-locked lasers, noise-induced transitions, optimal path, rare events, stochasticity, epidemiology, bit error ratios.

AMS subject classifications.

1. Introduction.

Recent years have seen a dramatic rise in the use of stochastic systems to model a wide variety of important physical and biological phenomena. Studies of sub-cellular processes and tissue dynamics [85], large-scale population dynamics [74], genetic switching [7], magnetic devices [57], optical devices[51, 81, 75, 20], Josephson junctions [37], fluid mechanics[34, 33, 48], weather and climate[87], and geosciences[82] have included numerous investigations into how noise affects physical and biological phenomena at a wide variety of scales. One often sees rare transition events in these systems that are induced by noise which may be internal or external to the system. These noise-induced rare events may be associated with a desirable outcome, such as the extinction of an infectious disease outbreak [6, 11] or eradication of a pest [71], or an undesirable outcome, such as the sudden clustering of cancerous cells [55], the outbreak of an infectious disease [72], or a bit error in a digital communication system [29]. Another important class of systems are those that exhibit rare events due to intermittently activated finite-time instabilities [64, 30]. These types of rare events include freak water waves in the ocean [17] and ship rolling and capsizing [65]. The need to understand these phenomena has fueled a demand for methods that quantify the impact of noise on complex systems.

In these stochastic systems, noise can affect the system in a variety of ways. Assessing the full impact of noise is rarely possible due to the "curse of dimensionality". Analysis and computations must often concentrate on the most important noise-induced events, which include spontaneous switching between coexisting stable states, critical failure of a system, and nucleation of coherent structures. One important feature of interest when studying noise-induced transitions is the optimal transition pathway of escape from a metastable state either to another metastable state or to a stable (absorbing) state. We define the optimal path as the path that is most likely to occur among all possible paths, recognizing that this path may not be unique or even exist (i.e., belong to the set of admissible paths). For systems out of equilibrium such that detailed balance is not satisfied, knowledge of the optimal

---

*Department of Mathematical Sciences, Montclair State University, Montclair, NJ 07043, USA (eric.forgoston@montclair.edu).

†Department of Mathematical Sciences, New Jersey Institute of Technology, Newark, NJ 07102, USA (rmoore@njit.edu).

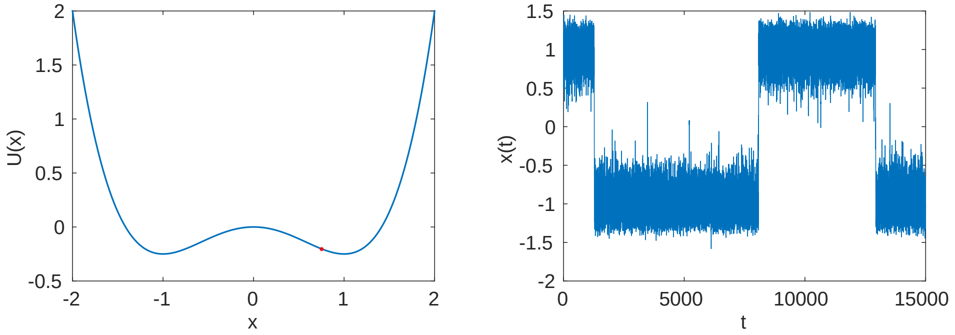

Fig. 1. *(a)Particle moving in a potential well under the influence of external noise. (b)Stochastic realization of the particle position in time.*

path is required for the computation of the mean switching time between states or the mean time to exit.

This article provides a tutorial overview of noise-induced rare events. By providing theoretical and numerical background along with several example applications of recently developed methods to compute the most likely noise pathways to critical events, we hope to enable the reader to quickly apply the methods to original applications of interest.

1.1. Noise sources. Stochasticity manifests itself as either external or internal noise. External noise comes from a source outside the system being considered (e.g. population growth under the influence of climatic effects, or a random signal fed into a transmission line), and often is modeled by replacing an external parameter with a random process. Internal noise is inherent to the system itself and is caused by the random interactions of discrete particles (e.g. individuals in a population, or molecules undergoing a chemical reaction) [44, 39, 86, 84]. Both types of noise can lead to a rare switching event between metastable states or a rare escape event from a metastable state.

Figure 1(a) shows a snapshot in time of a particle moving in a quartic potential well under the influence of external noise. Figure 1(b) shows a single realization of the particle position in time. One sees multiple rare stochastic switches from one well to another. Figure 2 shows a single realization of the population size in time for an Allee effect [2] problem in population biology. In this example, the noise is internal and arises from the random interactions of individuals in a population. One sees the population fluctuating about the carrying capacity for a long period of time until the rare extinction event occurs.

There are many possible escape/switching paths, but there is a path along which switching or escape is most likely to occur. We call this most likely path of escape or switching the optimal path. It is of great importance in a variety of applied problems to determine this optimal path since knowledge of the path then enables the determination of the mean time to escape from a metastable state or to switch from one metastable state to another metastable state.

Mathematically, the effect of external noise is often described using a Langevin equation or the associated Fokker-Planck equation (though the dynamics of external noise may sometimes be described by a master equation [78]). Feynman famously pointed out that each noise realization corresponds to a particular trajectory of the

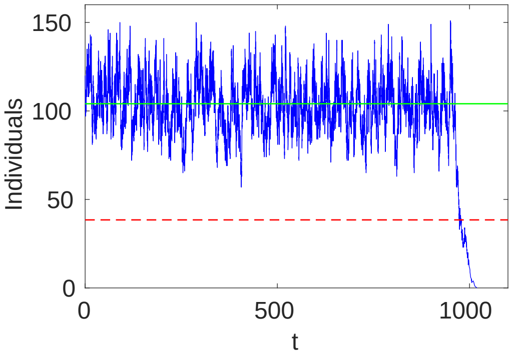

FIG. 2. *Stochastic realization of the population size in time where the local dynamics of the population exhibit the Allee effect. The green, solid line denotes the carrying capacity, while the red, dashed line denotes the Allee threshold.*

system, and therefore the probability density of realizations of trajectories is determined by the probability density of noise realizations [31]. This idea can be used to formulate a variational problem to find the optimal path that ultimately reduces to considering trajectories of an auxiliary Hamiltonian dynamical system. One can solve for the Hamiltonian dynamics, either analytically or numerically, for the most probable (i.e., optimal) path of escape or switching [36, 25].

The effect of internal noise due to the random interactions of individuals within the system is described mathematically using a master equation. The master equation is a large, or even infinite, set of differential equations that cannot in general be solved analytically. However, the optimal fluctuation path is found to solve an eikonal equation obtained via Wentzel-Kramers-Brillouin-Jeffreys (WKBJ) analysis of the master equation in the limit of weak internal noise [60, 38, 25, 28, 54, 6, 32, 80, 71, 11, 72]. As in the case of external noise, the optimal path is found by transforming the original stochastic problem into a new deterministic system described by a Hamiltonian $\mathcal{H}(x, \lambda)$. The dimension of the Hamiltonian is twice the dimension of the original system due to the conjugate momentum variables λ. An optimal path starting at a metastable state is identified with $\mathcal{H}(x, \lambda) = 0$; therefore, the method amounts to finding a zero-energy trajectory of an effective mechanical system, and at least one of the solutions to the zero-energy Hamiltonian is the optimal path. There may be other escape, switching, or extinction paths, but the optimal path is the path that maximizes the probability of escape, switching, or extinction [10].

1.2. Infinite-dimensional equations and large deviation theory. Even though it is often straightforward to extend the framework discussed in this article to infinite-dimensional systems with states defined on Hilbert spaces [18], we generally restrict our discussion to finite-dimensional examples. The exception to this is the formal introduction of stochastic PDEs used to model mode-locked lasers and communication systems introduced in Sections 3.1 and 3.2. The simulations performed in these sections, particularly those using importance sampling applied to (95), effectively limited the bandwidth of noise that was otherwise taken to be delta-correlated in both time and space. To the authors' knowledge no proof of well-posedness exists for this equation, and indeed when $c_2 = 0$ in (95), there is evidence to suggest that the stochastic PDE is ill-posed [14, 15].

Finally, we note that large deviation results for stochastic PDEs are becoming more common in the literature, particularly in the context of parabolic equations with damping at high wavenumbers [46, 45] Large deviation principles for the nonlinear Schrödinger equation with additive and multiplicative noise have been shown when the noise is colored in space [19, 40, 41].

2. Transitions, exits, and extinctions.

2.1. Mean first exit time due to external noise. The effect of noise on a physical system can be described in a variety of ways, all of which aim to capture how a single deterministic solution has been transformed by noise into a distribution of solutions and what the characteristics are of that distribution. This can take the form of a boundary value problem with random data or random coefficients, as one might find in the forward (scattering) problem associated with imaging of the earth or of living tissue, or it can take the form of an initial value problem with random data, as one might find in numerical weather prediction. We will focus here on initial value problems with time-dependent random forcing, specifically on stochastic dynamical systems described by a well-defined state evolving in time, where the evolution is probabilistic due to the presence of noise. This section provides some definitions to set the context of what follows. Although we will consider a one-dimensional (1D) framework, one can naturally extend the results to the multi-dimensional case.

We begin by considering the stochastic differential equation (SDE) described by

$$\dot{x} = f(x) + \eta(t), \tag{1}$$

where $\eta(t)$ expresses an additive randomly distributed noise term influencing the state $x(t)$. Whether resulting from truly random (e.g., quantum) phenomena or simply an assortment of physical phenomena not included in the model for reasons of scale or uncertainty, $\eta(t)$ can often be equated with the formal time derivative of a Brownian motion, resulting in paths $x(t)$ that are continuous and Markovian (i.e., "memoryless"). Since these paths, referred to as diffusion processes, are generally not differentiable, it is helpful to consider the statistics of finite increments $\Delta\eta = \eta(t+\Delta t) - \eta(t)$. These increments are drawn from a Gaussian distribution with mean and variance given by

$$\mathbb{E}[\Delta\eta] = 0 \quad \text{and} \quad \mathbb{E}[(\Delta\eta)^2] = D\Delta t, \tag{2}$$

where $\mathbb{E}[\cdot]$ denotes the expectation or expected value of a quantity with respect to its distribution. A natural way to think of (1) is therefore as the limit of the Euler-Maruyama method [73], which is simply the expression of the comments above in the form of a numerical integration method to obtain $\Delta x = x(t + \Delta t) - x(t)$:

$$\Delta x = f(x(t))\Delta t + \Delta\eta. \tag{3}$$

Then (1) is understood as the limiting process as $\Delta t \to 0$, such that

$$\mathbb{E}[\eta(t)] = 0 \quad \text{and} \quad \mathbb{E}[\eta(t)\eta(t')] = D\delta(t - t'), \tag{4}$$

where D is the noise intensity. Details of the Euler-Maruyama method can be found in Appendix A.

Some of the SDEs considered in the following sections have state-dependent functions multiplying the random term, i.e.,

$$\dot{x} = f(x) + \sigma(x)\eta(t). \tag{5}$$

This expression is subject to interpretation depending on how one determines the limit described above. Two standard interpretations of this stochastic integral predominate, including the prepoint or Itô interpretation,

$$\int_t^{t+\Delta t} \sigma(x(s))\eta(s)\,ds \approx \sigma(x(t))\Delta\eta, \tag{6}$$

and the midpoint or Stratonovich interpretation,

$$\int_t^{t+\Delta t} \sigma(x(s))\eta(s)\,ds \approx \frac{1}{2}\left[\sigma(x(t)) + \sigma(x(t+\Delta t))\right]\Delta\eta. \tag{7}$$

The examples to follow will use only the Itô interpretation for simplicity, although for many physical models the Stratonovich interpretation is more appropriate [86].

Reflecting the fact that (1) is best understood as a distribution of paths determined by possible realizations of the random driving term $\eta(t)$, its solution can be alternatively expressed as a transition density $p(x,t|y,s)$, such that the probability of finding $x(t)$ in a measurable set Ω conditioned on $x(s)=y$ with $s \le t$ is given by

$$P(x(t)\in\Omega|x(s)=y) = \int_\Omega p(x,t|y,s)\,dx. \tag{8}$$

The time evolution of this transition density satisfies the forward Fokker-Planck equation,

$$\frac{\partial p}{\partial t} = -\frac{\partial}{\partial x}(fp) + \frac{1}{2}D\frac{\partial^2 p}{\partial x^2} \tag{9}$$

with initial condition $p(x,s|y,s)=\delta(x-y)$. Conditional expectations can then be computed against this density using

$$\overline{g}(y,t) = \mathbb{E}[g(x(t))|y,s] = \int g(x)p(x,t|y,s)\,dx, \tag{10}$$

or the quantity $\overline{g}(y,t)$ can be evolved directly using the backward Fokker-Planck equation,

$$\frac{\partial \overline{g}}{\partial t} = f(y)\frac{\partial \overline{g}}{\partial y} + \frac{1}{2}D\frac{\partial^2 \overline{g}}{\partial y^2} \tag{11}$$

with initial condition $\overline{g}(y,s)=g(y)$.

An important application of the Fokker-Planck equation is in computing exit times of state x from a domain Ω. If we define g to be the indicator function associated with set Ω, $g(x)=\mathbb{1}_{x\in\Omega}$, then $\overline{g}(y,t)$ is the probability of being in Ω at time t having started at $x(0)=y$ (we set $s=0$ without loss of generality for time-homogenous processes). If we focus only on the first exit from Ω, we note that this probability satisfies (11) with absorbing boundary condition $\overline{g}|_{\partial\Omega}=0$ [39, 76]. Now we note that over a time interval $(t,t+\Delta t)$, the probability of exit from a trajectory starting at y is given by

$$\overline{g}(y,t) - \overline{g}(y,t+\Delta t) \approx -\frac{\partial \overline{g}}{\partial t}\Delta t. \tag{12}$$

In other words, $-\partial\overline{g}/\partial t$ is the exit time density. Under the assumption that all trajectories exit with probability one, the density can be used to compute the mean first exit time $\tau(y)$ for any $y \in \Omega$:

$$\tau(y) = \int_0^\infty t(-\frac{\partial \overline{g}}{\partial t})\, dt = \int_0^\infty \overline{g}(y,t)\, dt, \tag{13}$$

where we have integrated by parts and assumed that $t\overline{g} \to 0$ as $t \to \infty$. Integrating (11) thus yields a boundary value problem referred to as Dynkin's Equation for the mean first exit time [39],

$$f(y)\frac{\partial \tau}{\partial y} + \frac{1}{2}D\frac{\partial^2 \tau}{\partial y^2} = -1, \qquad \tau\,|_{\delta\Omega} = 0. \tag{14}$$

2.2. Large deviation theory, action and optimal paths. Section 2.1 poses two broad alternatives for computing expectations of functions of a diffusion process. The first is to solve the Fokker-Planck equation (9) using, for example, eigenfunction expansions (with an inner product defined with respect to a weighting that renders the operator self-adjoint). This approach is viable in one dimension as represented in (9), but quickly becomes numerically intractable if the state is high- or infinite-dimensional. This is partly due to the fact that, in the limit of small noise where $D \to 0$, the differential operator in (9) is singular. This feature implies the existence of boundary layers, rendering the computation numerically stiff. Analytically, the existence of a small parameter suggests the use of asymptotic methods such as singular perturbation or WKBJ theory to approximate the expectation [12, 63].

The second broad approach is to simulate the random walk in (1) multiple times and to compute the expectations empirically using, for example, a Monte Carlo method. The difficulty in using this approach for rare events in high-dimensional systems stems primarily from the fact that the desired expectation is dominated by a small set of events of interest. This problem is exacerbated in the small-noise limit due to an exponential drop-off in likelihood as the random walker moves away from this set. In this scenario of high dimension and small noise, it is thus critically important to bias the Monte Carlo simulations such that a substantial number of simulated trajectories coincide with those that sample from the set of interest with high likelihood. This search for a good bias function is made all the more important by the inherent inefficiency of the Monte Carlo method, which produces estimators with relative error that scales as $1/\sqrt{N}$ where N is the sample size of simulations. The importance of this issue has led to the development of many techniques appropriate for rare-event sampling in a variety of physical contexts [47, 88, 90, 1].

Regardless of whether one uses asymptotic methods to approximate an expectation or uses importance sampling to concentrate Monte Carlo simulations on states of interest, both approaches lead to the theory of large deviations described in detail in the text by Freidlin and Wentzell [36]. We will now present a description of this theory, focusing on providing a practical introduction to exit problems on finite and infinite time horizons.

We return to (1),

$$\dot{x} = f(x) + \eta(t), \tag{15}$$

where the noise $\eta(t)$ is as described in (4). Each noise realization $\eta(t)$ produces an associated trajectory $x(t)$. Therefore, the probability of generating a given path $x(t)$

is proportional to that of generating the corresponding noise realization $\eta(t)$ [31]. The formal probability density for this Gaussian noise process satisfies

$$P[\eta(t)] \propto \exp\left(-\frac{1}{2D}\int_{t_i}^{t_f} \eta^2\, dt\right). \tag{16}$$

Substitution of (15) into (16) gives [31, 24]

$$P[x(t)] \propto \exp\left(-\frac{1}{2D}\int_{t_i}^{t_f} (\dot{x} - f(x))^2\, dt\right). \tag{17}$$

Since we are concerned with maximizing this probability density over a set of eligible paths satisfying, for example, boundary conditions $x(t_i) = x_i$ and $x(t_f) = x_f$, we express (17) using the conventions of variational calculus, where

$$P[x(t)] \propto \exp\left(-\frac{1}{2D}\int [\dot{x} - f(x)]^2\, dt\right) \propto \exp\left(-\mathcal{S}[x(t)]/D\right), \tag{18}$$

with action $\mathcal{S}$ and Langrangian $\mathcal{L}$ [35, 24, 36, 62] defined by

$$\mathcal{S}[x(t)] = \int_{t_i}^{t_f} \mathcal{L}(\dot{x}, x; t)\, dt, \qquad \mathcal{L}(\dot{x}, x; t) = \frac{1}{2}[\dot{x} - f(x)]^2. \tag{19}$$

Next, we calculate the probability of a transition between two states. In the limit as $D \to 0$, this probability will be increasingly dominated by the path that minimizes $\mathcal{S}[x(t)]$ so that $P[x(t)]$ is a maximum. This optimal fluctuational path x_{opt} is found as a solution to the variational problem $\delta\mathcal{S}[x] = 0$, where

$$\delta\mathcal{S}[x] = \mathcal{S}[x + \delta x] - \mathcal{S}[x] = \int_{t_i}^{t_f} \mathcal{L}(\dot{x} + \delta\dot{x}, x + \delta x; t)\, dt - \int_{t_i}^{t_f} \mathcal{L}(\dot{x}, x; t)\, dt$$

$$= \int_{t_i}^{t_f} \left[\frac{\partial \mathcal{L}}{\partial x} - \frac{d}{dt}\left(\frac{\partial \mathcal{L}}{\partial \dot{x}}\right)\right] \delta x\, dt = 0. \tag{20}$$

Since the variation δx is arbitrary one is left with the Euler-Lagrange equation

$$\frac{\partial \mathcal{L}}{\partial x} - \frac{d}{dt}\left(\frac{\partial \mathcal{L}}{\partial \dot{x}}\right) = f(x)f'(x) - \ddot{x} = 0, \tag{21}$$

which is then solved for the optimal path x_{opt}. It is worth noting that the optimal path has been found by transforming the original stochastic problem into a new deterministic system described by the Euler-Lagrange equation (21). The dimensions of the Euler-Lagrange equation are twice the dimensions of the original system.

Following the standard progression of classical mechanics, it is sometimes of use to move from the Lagrangian $\mathcal{L}$ expressed in terms of the state x and associated velocity $\dot{x}$ to the Hamiltonian $\mathcal{H}$ formulated as a function of x and the conjugate momentum λ defined as

$$\lambda = \frac{\partial \mathcal{L}}{\partial \dot{x}} = \dot{x} - f(x). \tag{22}$$

Note that we are denoting the conjugate momentum variable as λ rather than the usual p to avoid conflict with our use of p for probability density and to emphasize the connection between conjugate momentum and the costate (i.e., Lagrange multiplier) from the optimal control formulation below. One way to move from the Lagrangian $\mathcal{L}$ to the Hamiltonian $\mathcal{H}$ is through the Legendre transformation

$$\mathcal{L} = \lambda \dot{x} - \mathcal{H}(x, \lambda), \tag{23}$$

where $\dot{x}$ is found as a function of x and λ from $\lambda = \frac{\partial \mathcal{L}}{\partial \dot{x}}$ using the inverse function theorem. Starting with (1), the Legendre transformation yields

$$\dot{x} = f(x) + \lambda, \quad \text{and} \quad \mathcal{H} = \frac{\lambda^2}{2} + \lambda f(x), \tag{24}$$

illustrating the connection between the classical momentum λ and the optimal fluctuation η.

One can then write the action $\mathcal{S}$ as

$$\mathcal{S}[x(t)] = \int_{t_i}^{t_f} \mathcal{L}(\dot{x}, x; t)\, dt = \int_{t_i}^{t_f} \left(\lambda \dot{x} - \mathcal{H}(x, \lambda)\right)\, dt. \tag{25}$$

The optimal path is found as a solution to the variational problem $\delta \mathcal{S}[x, \lambda] = 0$, where variations in both x and λ must be considered. This leads to

$$\begin{aligned} \delta \mathcal{S}[x, \lambda] &= \mathcal{S}[x + \delta x, \lambda + \delta \lambda] - \mathcal{S}[x, \lambda] \\ &= \int_{t_i}^{t_f} \left[(\lambda + \delta\lambda)(\dot{x} + \delta\dot{x}) - \mathcal{H}(x + \delta x, \lambda + \delta\lambda)\right] dt - \int_{t_i}^{t_f} \left[\lambda \dot{x} - \mathcal{H}(x, \lambda)\right] dt \\ &= \int_{t_i}^{t_f} \left[\left(\dot{x} - \frac{\partial \mathcal{H}}{\partial \lambda}\right) \delta\lambda - \left(\dot{\lambda} + \frac{\partial \mathcal{H}}{\partial x}\right) \delta x\right] dt = 0. \end{aligned} \tag{26}$$

As with the Lagrangian formulation, both variations are arbitrary. Therefore one is left with Hamilton's equations

$$\dot{x} = \frac{\partial \mathcal{H}}{\partial \lambda}, \qquad \text{and} \qquad \dot{\lambda} = -\frac{\partial \mathcal{H}}{\partial x}. \tag{27}$$

To avoid potential inverse function theorem issues, one could find the Hamiltonian from the outset. Thus,

$$P[\eta(t)] \propto \exp\left(-\frac{1}{2D} \int_{t_i}^{t_f} \eta^2\, dt\right) = \exp(-\mathcal{R}_\eta / D) \quad \text{and} \quad \mathcal{R}_\eta[\eta(t)] = \frac{1}{2} \int_{t_i}^{t_f} \eta^2\, dt, \tag{28}$$

where we regard R_η as an objective function. To find the optimal trajectory, one must minimize the functional

$$\mathcal{R}[x, \eta, \lambda] = \mathcal{R}_\eta[\eta(t)] + \int_{t_i}^{t_f} \lambda[\dot{x} - f(x) - \eta(t)]\, dt, \tag{29}$$

where λ is the Lagrange multiplier enforcing the dynamic constraint (1). Therefore

$$P[x(t)] \propto \exp(-R/D), \tag{30}$$

where the value R is obtained from

$$R = \min \mathcal{R}[x, \eta, \lambda]. \tag{31}$$

We extremize $\mathcal{R}[x, \eta, \lambda]$ with respect to η, λ, and x as follows:

$$\frac{\delta \mathcal{R}}{\delta \eta} = \mathcal{R}[x, \eta + \delta\eta, \lambda] - \mathcal{R}[x, \eta, \lambda] = \int_{t_i}^{t_f} (\eta - \lambda)\delta\eta \, dt = 0, \tag{32}$$

so that

$$\lambda = \eta; \tag{33}$$

$$\frac{\delta \mathcal{R}}{\delta \lambda} = \mathcal{R}[x, \eta, \lambda + \delta\lambda] - \mathcal{R}[x, \eta, \lambda] = \int_{t_i}^{t_f} (\dot{x} - f(x) - \eta(t))\delta\lambda \, dt = 0, \tag{34}$$

so that

$$\dot{x} = f(x) + \eta(t); \qquad \text{and} \tag{35}$$

$$\frac{\delta \mathcal{R}}{\delta x} = \mathcal{R}[x + \delta x, \eta, \lambda] - \mathcal{R}[x, \eta, \lambda] = \int_{t_i}^{t_f} (-\dot{\lambda} - \lambda \frac{\partial f}{\partial x})\delta x \, dt = 0, \tag{36}$$

so that

$$\dot{\lambda} = -\lambda \frac{\partial f}{\partial x}. \tag{37}$$

Taken together we have

$$\dot{x} = f(x) + \lambda, \quad \dot{\lambda} = -\lambda \frac{\partial f}{\partial x}, \quad \text{and} \quad \mathcal{H}(x, \lambda) = \frac{\lambda^2}{2} + \lambda f(x). \tag{38}$$

By comparison with the Lagrangian formulation, it is clear that the Lagrange multiplier plays the role of the conjugate momentum.

As mentioned in Sec. 1.1, in both formulations the optimal path is found by transforming the original stochastic problem into a new deterministic system described by a Hamiltonian with $\mathcal{H}(x, \lambda) = 0$ when x_i is a metastable state and $t_i = -\infty$. The dimensions of the Hamiltonian are twice the dimensions of the original system due to the conjugate momenta λ. The method amounts to finding a zero-energy trajectory of an effective mechanical system, and at least one of the solutions to the zero-energy Hamiltonian is in the set of optimal paths.

2.3. Escape in finite and infinite time. In Sec. 2.2 we formulated a criterion satisfied by optimal (i.e., most likely) diffusion paths produced by (1). These paths must also satisfy time constraints and boundary conditions reflecting, for example, a transition between quasi-stable states either in finite time or over an arbitrarily long time. The minimal action and associated paths strongly depend on the time horizon relevant to the computations. Computing mean first exit times from Ω generated by (5) requires minimizing the following action over all exit times t_f:

$$\mathcal{S}_{t_\mathrm{f}} = \frac{1}{2}\int_{t_\mathrm{i}}^{t_\mathrm{f}} (\dot{x} - f(x))^\dagger a^{-1}(x)(\dot{x} - f(x))\, dt, \tag{39}$$

where we generalize the presentation in Sec. 2.1 to higher dimension so that $x \in \mathbb{R}^n$ and $a(x) = \sigma(x)\sigma^\dagger(x)$. Performing this minimization over paths from points x_i to x_f yields the function

$$Q(x_\mathrm{i}, x_\mathrm{f}) = \inf_{t_\mathrm{f}} \mathcal{S}_{t_\mathrm{f}}[x(t)|x(t_\mathrm{i}) = x_\mathrm{i}, x(t_\mathrm{f}) = x_\mathrm{f}], \tag{40}$$

known as the quasi-potential for its similarity in form to a potential defined between any two points. Indeed, in the case of overdamped Langevin dynamics [58, 77, 39, 86] when (5) is a noise-driven gradient flow so that

$$f(x) = -\left(\frac{\partial U}{\partial x}\right)^\dagger, \tag{41}$$

the quasi-potential is intimately related to the potential U, and under additional assumptions $Q(x_\mathrm{i}, x_\mathrm{f}) = 2(U(x_\mathrm{f}) - U(x_\mathrm{i}))$. Regardless of whether f is a gradient, the quasi-potential determines the scaling law of exit rates $\tau(x) := \inf\{t : X_t \notin \Omega | X_i = x\}$ as $D \to 0$, with

$$\mathbb{E}[\tau(x)] \sim \exp\left(\inf_{y\notin\Omega} Q(x,y)/D\right).$$

SDEs with sufficient complexity require a numerical approach to compute the quasi-potential [13], starting either from the optimal control formulation in (29) or from the Hamiltonian framework presented in (27). To include the matrix $a(x)$ in (39), assumed positive-definite to reflect a non-degenerate noise process in (5), the Hamiltonian is changed slightly to

$$\mathcal{H}(x, \lambda) = \frac{1}{2}\lambda^\dagger a \lambda + \lambda^\dagger f. \tag{42}$$

Finite-time paths can then be solved using a shooting method to solve the two-point boundary value problem expressed by

$$\dot{x} = f(x) + a\lambda \quad \text{and} \tag{43}$$

$$\dot{\lambda} = -\left(\frac{\partial f}{\partial x}\right)^\dagger \lambda - \frac{1}{2}\left[\frac{\partial}{\partial x}(\lambda^\dagger a \lambda)\right]^\dagger, \tag{44}$$

where we have used the convention of representing vectors as columns and derivatives with respect to those vectors as rows. Given a typical exit problem with fixed initial condition x_i and exit criterion forcing $x(t_\mathrm{f})$ to lie on the boundary $\partial\Omega$ of set Ω, for instance, a straightforward shooting method would start with an initial guess for λ

(e.g., $\lambda(t) \equiv 0$), integrate (43), adjust $\lambda(t_{\mathrm{f}})$ and integrate (44) backwards, then iterate this process until the terminal condition is satisfied [16, 28].

Different alternatives exist for finding optimal paths in the case of gradient systems, including the nudged elastic band method [52] and the string method [27]. A powerful method for more general dynamical systems is the minimum action method (MAM), which can be adapted via a rescaling in time to accommodate infinite-time optimal paths, e.g., where either $t_i = -\infty$ in (39) or (40) or the minimization over t_f in those expressions yields $t_f = \infty$. It sets up the minimization as the gradient descent of the action $\mathcal{S}_{t_{\mathrm{f}}}$. This can be accomplished in a number of ways, including by differentiating out the dependence of Hamilton's equations on the quasi-momentum λ and advancing a PDE whose steady state is the optimal path sought. The adaptation of this method to infinite-time problems, referred to as the geometric minimum action method (GMAM) [49], reparameterizes the optimal path to depend on arclength rather than time, removing the obvious difficulty of enforcing boundary conditions at infinity. The iterative action minimization method (IAMM) is a similar method that employs a direct, fully explicit iterative scheme [61]. Basic details of both the GMAM and the IAMM can be found in Appendix B.

2.3.1. Escape from potential well. As an example of an infinite-time calculation, consider a particle in a potential well under the influence of external Gaussian noise. The noise causes the particle to escape from the well in which it resides, an event that grows increasingly rare as the strength of the noise decreases. To determine the mean time to escape (MTE) in this limit, we consider again the Langevin equation

$$\dot{x} = -\frac{\partial U}{\partial x} + \eta(t), \tag{45}$$

where x is the particle's position, U determines the potential well, and η is additive Gaussian noise as described by (4). The associated Fokker-Planck equation is

$$\frac{\partial p(x,t)}{\partial t} = \frac{\partial}{\partial x}\left[\frac{\partial U(x)}{\partial x} p(x,t)\right] + \frac{1}{2} D \frac{\partial^2 p(x,t)}{\partial x^2}, \tag{46}$$

where p is the probability density. The first term on the right-hand side is the drift or transport term, and the second term on the right-hand side is the diffusion or fluctuation term. It is possible to rewrite (46) as

$$\frac{\partial p}{\partial t} = -\frac{\partial J}{\partial x}, \qquad J = -\frac{\partial U}{\partial x} p - \frac{1}{2} D \frac{\partial p}{\partial x}. \tag{47}$$

Therefore, $\frac{\partial p}{\partial t} + \frac{\partial J}{\partial x} = 0$ is a continuity equation for the probability density p, and J is interpreted as a probability current. For a stationary process, $J =$ constant.

Figure 3 shows a schematic of a potential well $U(x)$. We assume the well height is much larger than the noise intensity so that $\Delta U/D \gg 1$. We will determine the escape rate/time for particles sitting in a deep well near $x = x_{\min}$.

The probability current given by (47) can be rewritten as

$$J = -\frac{1}{2} D \exp\left(-2U(x)/D\right) \frac{\partial}{\partial x}\left[\exp\left(2U(x)/D\right) p(x,t)\right]. \tag{48}$$

Integration from $x_{\min}$ to A gives, under the assumption of quasi-stationarity (i.e., J

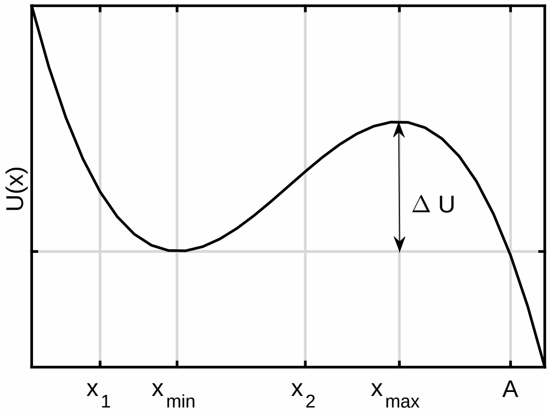

FIG. 3. *Schematic of a potential well $U(x)$. The local minimum of the well is located at $x = x_{\min}$, while the top of the barrier is located at $x = x_{\max}$.*

is constant),

$$J = \frac{D \exp\left(2U(x_{\min})/D\right) p(x_{\min}, t)}{2 \int_{x_{\min}}^{A} \exp\left(2U(x)/D\right) dx}, \tag{49}$$

where $x = A$ is the location of an arbitrary point far to the right of the location of the top of the well barrier (see Fig. 3). For a high barrier the quasi-stationary distribution of the Fokker-Planck equation satisfies

$$0 \approx \frac{\partial}{\partial x}\left[\frac{\partial U(x)}{\partial x} p(x,t)\right] + \frac{1}{2} D \frac{\partial^2 p(x,t)}{\partial x^2}, \tag{50}$$

where the time dependence of $p(x,t)$ arises from a slow leakage of probability from the well. The quasi-stationary distribution function near $x_{\min}$ is then

$$p(x,t) = p(x_{\min}, t) \exp\left(-2[U(x) - U(x_{\min})]/D\right). \tag{51}$$

The probability $P(t)$ to find the particle in the well is

$$P = \int_{x_1}^{x_2} p(x,t)\, dx = p(x_{\min}, t) \exp\left(2U(x_{\min})/D\right) \int_{x_1}^{x_2} \exp\left(-2U(x)/D\right) dx, \tag{52}$$

where $x = x_1$ and $x = x_2$ are the locations of arbitrary points in the potential well found respectively to the left and the right of $x = x_{\min}$ (see Fig. 3). Since probability P times the escape rate r is the probability current J, the inverse escape rate (escape time) is

$$\tau = \frac{1}{r} = \frac{P}{J} = \frac{2}{D} \int_{x_1}^{x_2} \exp\left(-2U(x)/D\right) dx \int_{x_{\min}}^{A} \exp\left(2U(x)/D\right) dx. \tag{53}$$

The first integral is largest near $x_{\min}$. We expand

$$U(x) \approx U(x_{\min}) + \frac{1}{2} U''(x_{\min})(x - x_{\min})^2. \tag{54}$$

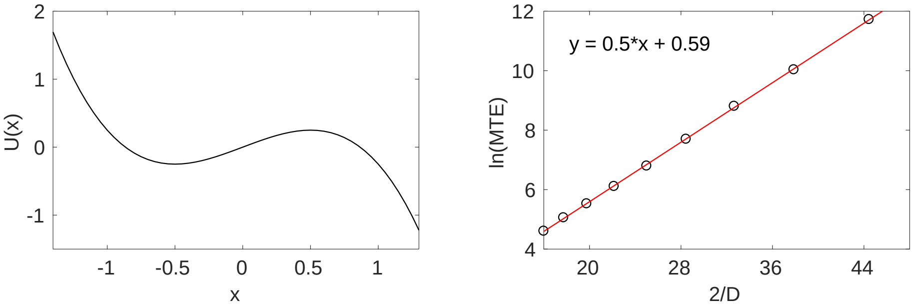

Fig. 4. *(a) Graph of the potential well given by* $U(x) = -x^3 + \frac{3}{4}x$ *with associated well height* $\Delta U = \frac{1}{2}$*. (b) Logarithm of the numerically computed mean time to extinction (black circles) as a function of* $2/D$ *with a line of best fit (red line) passing through the data. The equation of the best fit line is* $y = 0.5x + 0.59$*, whose slope agrees perfectly with the analytical prediction of* $\Delta U = \frac{1}{2}$*.*

The second integral is largest near $x_{\max}$. Again, we expand

$$U(x) \approx U(x_{\max}) - \frac{1}{2}|U''(x_{\max})|(x - x_{\max})^2. \tag{55}$$

By extending the integral boundaries to ±∞ in both directions, one obtains the expression for the MTE as

$$\tau = \frac{2\pi}{\sqrt{U''(x_{\min})|U''(x_{\max})|}} \exp\left(2[U(x_{\max}) - U(x_{\min})]/D\right) = K \exp\left(2\Delta U/D\right). \tag{56}$$

It is important to note in (56) that the escape time increases exponentially with increasing barrier height and decreasing noise intensity, and the prefactor K depends on the curvatures at $x_{\min}$ and $x_{\max}$.

A specific example is shown in Fig. 4(a)-(b). Figure 4(a) shows the potential well given by $U(x) = -x^3 + \frac{3}{4}x$ with associated barrier height $\Delta U = \frac{1}{2}$. We numerically integrate (45) using the Euler-Maruyama method (Appendix A), and the time needed for a particle to escape from the well is determined. By performing the computation for 10,000 particles, the mean time to escape is computed for a variety of noise intensities. By taking the logarithm of (56), one has $\ln \tau = \ln K + \frac{2\Delta U}{D}$. By plotting $\ln \tau$ versus $2/D$, the analytical prediction is that the data should lie along a line with slope $m = \Delta U$. Figure 4(b) shows the numerical results for the potential shown in Fig. 4(a) along with a line of best fit through the data. One can see excellent agreement between the numerical and analytical results.

Returning to the SDE description, the optimal fluctuation equations given by (27) are easily shown in the gradient case under consideration to give

$$\ddot{x} = \frac{\partial U}{\partial x}\frac{\partial^2 U}{\partial x^2}, \tag{57}$$

which integrates once to give

$$\dot{x}^2 = \left(\frac{\partial U}{\partial x}\right)^2 + c. \tag{58}$$

In the case of infinite-time exit, the constant $c = 0$, leading to an asymptotic dynamic behavior where the conjugate momentum λ is either zero or acts against the gradient,

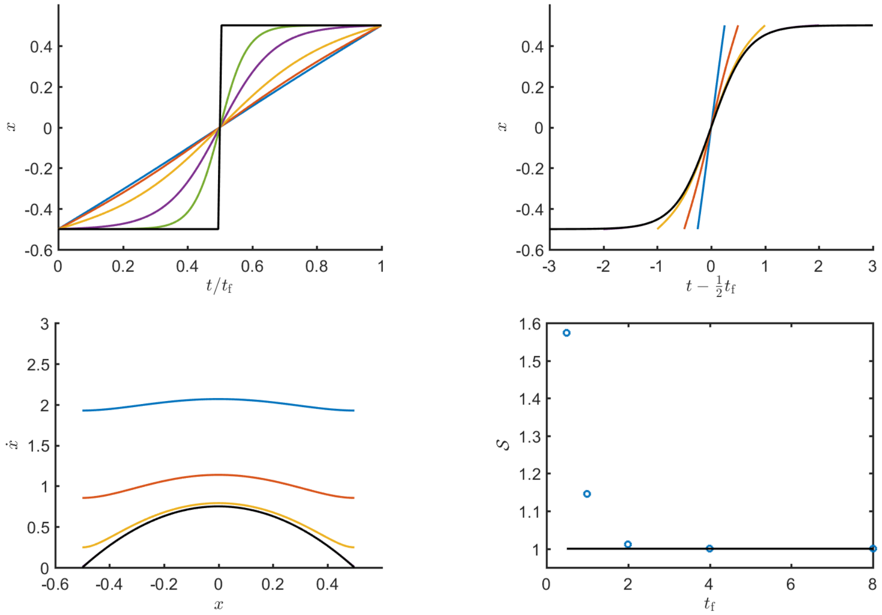

FIG. 5. *Optimal paths computed from the stable fixed point to the saddle for final times $t_\mathrm{f} = 1/2$ (blue), $t_\mathrm{f} = 1$ (red), $t_\mathrm{f} = 2$ (orange), $t_\mathrm{f} = 4$ (purple), $t_\mathrm{f} = 8$ (green) and $t_\mathrm{f} = \infty$ (black). (a) Top left: Optimal paths rescaled to unit exit time. (b) Top right: Optimal paths with time shifted so that passages through zero coincide. (c) Bottom left: Phase portrait ($\dot{x}$ vs. x). (d) Bottom right: Minimum action $\mathcal{S}$ vs. t_f.*

i.e.,

$$\dot{x} = -\frac{\partial U}{\partial x} + \lambda = \mp\frac{\partial U}{\partial x}, \tag{59}$$

depending on whether or not the uncontrolled dynamics (i.e., the deterministic dynamics obtained by setting $\eta \equiv 0$ in (45)) leads x in the direction of an exit. If $x(t_\mathrm{i}) < -1/2$, the uncontrolled dynamics takes infinite time to descend into the stable fixed point, after which the controlled dynamics follows the trajectory

$$x(t) = \frac{1}{2}\tanh(\frac{3}{2}t), \tag{60}$$

taking infinitely long both to rise out of the stable fixed point and to approach the saddle, thereby effecting an exit. The minimum action for any initial condition to the left of the stable fixed point is $\mathcal{S} = 2\Delta U = 1$.

To see how this changes when a finite time horizon is imposed, note that in this case (57) no longer implies (59). Figures 5(a)-(d) show the optimal paths and their phase portraits associated with $t_\mathrm{f} \in \{1/2, 1, 2, 4, 8\}$ and compares them to the infinite-time optimal path. Whereas for short time $t_\mathrm{f} = 1/2$ the optimal path is near a straight line path (more generally, a geodesic with respect to the metric imposed by $a(x)$), the optimal path quickly approaches the infinite-time path as t_f increases. Once these paths are indistinguishable, i.e., by $t_\mathrm{f} = 4$, increases in t_f simply add to the time spent vanishingly close to either fixed point. By this value of t_f, the action has also converged to its quasi-potential value of $\mathcal{S} = Q(-1/2, 0) = 1$. The phase portrait depicted in Fig. 5(c) demonstrates again that for short times t_{f} the optimal path tends to a constant velocity that generates the straight-line path depicted in Fig. 5(b); however, for large times the path through phase space collapses onto the anti-gradient flow described above.

Finally, we note that the reference to "infinite-time optimal paths" implies passage from, to, or through a hyperbolic fixed point. The optimization suggested by (39) performed on paths connecting two points that are not hyperbolic fixed points of the dynamical system and that do not pass through one, e.g., $x(t_{\mathrm{i}}) = -1/4$ and $x(t_{\mathrm{f}}) = 1/4$, yields an action determined by the quasi-potential $Q = 2\Delta U = 11/16$ and an optimal path time of

$$\Delta t = \frac{4}{3}\tanh^{-1}\frac{1}{2} = 0.73. \tag{61}$$

2.4. Master equation formalism for internal noise. Just as we considered the mean exit time due to external noise in Sec. (2.1), we would like to determine the mean time to extinction (MTE) and the optimal path for internal noise. Assuming again that we can model stochastic population dynamics using a Markov process, we describe the evolution of the probability density using the master equation

$$\frac{\partial \rho(X,t)}{\partial t} = \sum_r \left[W_r(X-r)\rho(X-r,t) - W_r(X)\rho(X,t)\right], \tag{62}$$

where $\rho(X,t)$ is the probability of finding X individuals at time t, and $W_r(X)$ is the transition rate from X to $X+r$, where r is a positive or negative integer increment. The first term of (62) is the gain to state X from state $X-r$. The second term of (62) is the loss from state X to other states.

The master equation is a large, or even infinite, set of differential equations. A diffusion approximation leading to a Fokker-Planck equation as in (9) is often used but is very (exponentially) inaccurate [42, 21, 54, 5]. Assuming that the typical size of the population $X \sim K$ as determined by the maximum of the quasi-stationary probability distribution, we can use a WKBJ approximation of the master equation [60, 38, 25, 28, 54]. If the mean-field equation associated with the original stochastic problem is n-dimensional, then the WKBJ method transforms the problem into one of classical mechanics in $2n$-dimensional phase space where the doubling of dimension is due to the conjugate momenta. It is important to note that these deterministic dynamics are not the system size $K \to \infty$ mean-field dynamics of the original stochastic model, but rather provide auxiliary dynamics that describe processes not captured by the mean-field dynamics.

For large populations, the time to extinction is long. The mean time to extinction is determined by the probability flux (extinction rate) into the extinct state, and is determined by the tail of the quasi-stationary probability distribution where $\frac{\partial \rho}{\partial t} \approx 0$. Therefore

$$0 = \sum_r \left[W_r(X-r)\rho(X-r) - W_r(X)\rho(X)\right]. \tag{63}$$

Let X be scaled by K, the typical population size in the metastable state. Using $x = X/K$, the transition rate $W_r(X) = W_r(Kx)$ can be represented as the following expansion in K,

$$W_r(Kx) = Kw_r(x) + u_r(x) + \mathcal{O}(1/K), \tag{64}$$

where x and the scaled transition rates w_r and u_r are $\mathcal{O}(1)$. Additionally we can write,

$$\rho(X) \equiv \rho(Kx) = \pi(x). \tag{65}$$

Then the scaled master equation is

$$\sum_r \Big[w_r(x - \frac{r}{K})\pi(x - \frac{r}{K}) - w_r(x)\pi(x) \Big] = 0. \tag{66}$$

For $K \gg 1$ we approximate the scaled master equation using the WKB approximation. To apply the WKB approximation, we assume that

$$\pi(x) = A(x) \exp\left[(-K\mathcal{S}(x))(1 + \mathcal{O}(1/K))\right]. \tag{67}$$

We substitute the WKB ansatz along with $\mathcal{S}(x - \frac{r}{K}) = \mathcal{S}(x) - \frac{r}{K}\mathcal{S}'(x) + \frac{r^2}{2K^2}\mathcal{S}''(x) + \mathcal{O}(1/K^3)$ and $A(x - \frac{r}{K}) = A(x) - \frac{r}{K}A'(x) + \mathcal{O}(1/K^2)$ into the master equation, and at leading order one obtains a Hamilton-Jacobi equation with Hamiltonian

$$\mathcal{H}(x, \lambda) = \sum_r w_r(x)[\exp{(r\lambda)} - 1] = 0, \qquad \lambda = \frac{\partial \mathcal{S}}{\partial x}. \tag{68}$$

Hamilton's equations are

$$\dot{x} = \frac{\partial \mathcal{H}}{\partial \lambda} = \sum_r r w_r(x) \exp{(r\lambda)}, \tag{69a}$$

$$\dot{\lambda} = -\frac{\partial \mathcal{H}}{\partial x} = -\sum_r [\exp{(r\lambda)} - 1] \frac{\partial w_r(x)}{\partial x}. \tag{69b}$$

In summary, the WKB solution amounts to finding a zero-energy trajectory of an effective mechanical system, and at least one of the solutions to the zero-energy Hamiltonian is the optimal path. The x dynamics along the $\lambda = 0$ deterministic line are described by

$$\dot{x} = \frac{\partial \mathcal{H}(x, \lambda)}{\partial \lambda}|_{\lambda=0} \tag{70}$$

which is the rescaled mean-field rate equation associated with the original deterministic problem. For a single step process, this simplifies to $\dot{x} = w_1(x) - w_{-1}(x)$.

In Sec. 3.3, we will discuss the application of this master equation formalism to two examples involving extinction in population biology. For the simple models discussed in Sec. 3.3, the deterministic steady states are nodes. It is easy to show that the WKB method transforms these steady state nodes in the original 1D deterministic system into steady state saddle points in the 2D set of Hamilton's equations. This allows for noise-induced escape from a metastable state and provides a path to extinction that did not exist in the original deterministic model.

2.5. Mean Time to Extinction. In a single step process, such as the two examples considered in Sec. 3.3, the optimal path $\lambda_{opt}(x)$ will always have the general form

$$\lambda_{opt}(x) = -\ln{(w_{+1}(x)/w_{-1}(x))}. \tag{71}$$

Using the definition of the conjugate momentum $\lambda = d\mathcal{S}/dx$, the action $\mathcal{S}_{opt}$ along the optimal path $\lambda_{opt}(x)$ is given by

$$\mathcal{S}_{opt} = \int^{x} \lambda_{opt}(x)dx, \tag{72}$$

where the limits of integration are determined by the appropriate equilibrium points of the specific problem. Therefore, the mean time to extinction (MTE) can be approximated by

$$\tau = B\exp(K\mathcal{S}_{opt}), \tag{73}$$

where B is a prefactor that depends on the system parameters and on the population size. An accurate approximation of the MTE depends on obtaining B. The specific form of the prefactor differs for the two types of extinction problems considered in Sec. 3.3, and are provided in that section.

2.6. Sampling for exits. In the simple gradient flow discussed in Sec. 2.3.1 it is possible to obtain or approximate not only the exponential scaling law in D of the exit probability over finite times, but also the normalization constant that provides the pre-exponential factor K in (56). In flows that are more complex, including non-potential flows that do not satisfy detailed balance [86] and those of higher (or infinite) dimension, this is no longer possible analytically. Nor is it practical computationally, due to the formation of boundary layers with the singular perturbation introduced as $D \to 0$ in Dynkin's equation (14) or the time-dependent Fokker-Planck equation (9).

An alternate method to obtain the normalization constant uses sampling through Monte Carlo simulations. This too is subject to the "curse of dimensionality" in cases of high dimension such as discretizations of stochastic PDEs; however, variance reduction techniques can be used to improve the numerical efficiency of obtaining an estimate. We will focus here on importance sampling, a variance reduction method that uses information from the controlled dynamics of the deterministic system to inform a bias applied to the distribution from which the Monte Carlo simulations are drawn.

Suppose we wish to calculate the probability that, after time t_{f}, a stochastic process $x(t)$ evolving according to (5) terminates outside of set Ω, i.e., with $x(t_{\mathrm{f}}) \notin \Omega$, where we assume for concreteness that the deterministic evolution $\dot{x} = f(x,t)$ yields $x(t) \in \Omega$ for $x(t_{\mathrm{i}}) = x_{\mathrm{i}}$ and $t \leq t_{\mathrm{f}}$. In other words, we wish to calculate the probability that the stochastic forcing term $\sigma(x,t)\eta$ drives the state some distance away from its deterministic trajectory. The standard Monte Carlo estimator for this probability P is given by

$$\hat{P}_{\mathrm{MC}} = \frac{1}{N}\sum_{k=1}^{N} I(X_{t_{\mathrm{f}}}^{(k)}) \tag{74}$$

where $\{X_{t_{\mathrm{f}}}^{(k)}, k = 1, \ldots, N\}$ are N independent simulations of (1) and $I(x)$ is an indicator function evaluating to 0 if $x \in \Omega$ and 1 otherwise. Thus, $I(X_{t_{\mathrm{f}}})$ forms a Bernoulli random variable, implying that the estimator $\hat{P}_{\mathrm{MC}}$ has variance given by

$$\mathbb{V}\Big[\hat{P}_{\mathrm{MC}}\Big] = \frac{P(1-P)}{N}, \tag{75}$$

with a relative error (coefficient of variation) of,

$$\mathbb{C}_{\mathrm{var}}\left[\hat{P}_{\mathrm{MC}}\right] = \frac{\sqrt{\mathbb{V}\left[\hat{P}_{\mathrm{MC}}\right]}}{\mathbb{E}\left[\hat{P}_{\mathrm{MC}}\right]} = \frac{\sqrt{1-P}}{\sqrt{NP}}. \tag{76}$$

Ensuring that (74) is an accurate estimator for the true probability requires that $\mathbb{C}_{\mathrm{var}}\left[\hat{P}_{\mathrm{MC}}\right] \ll 1$. However, if the set Ω and noise strength D are such that $P \ll 1$ (i.e., $X_{t_{\mathrm{f}}} \notin \Omega$ is a rare event), this requirement is approximately expressed by $N \gg 1/P$, which implies that a very large (and often unattainable) number of Monte Carlo runs is required to obtain an accurate estimate.

The idea behind importance sampling for diffusions is to replace the original dynamics given by (5) with

$$\dot{x} = f(x,t) + \sigma(x,t)(b+\eta), \tag{77}$$

so that the noise term η is biased in such a way that the events of interest, $x(t_{\mathrm{f}}) \notin \Omega$, are much more likely. The particular form of bias suggested by (77) is mean-biasing; other forms of biasing the noise are possible but less common. Mean biasing effectively replaces increments $\Delta\eta$ drawn from the original distribution (e.g., Gaussian) $p(\Delta\eta)$ by shifted increments

$$\Delta\tilde{\eta} = \Delta\eta + b\Delta t, \tag{78}$$

which is equivalent to drawing $\Delta\tilde{\eta}$ from biased distribution $\tilde{p}(\Delta\tilde{\eta}) = p(\Delta\tilde{\eta} - b\Delta t)$. Despite the biased dynamics described by (77), an unbiased estimator can be recovered from Monte Carlo simulations of this equation through an appropriate weighting referred to as the likelihood ratio

$$l(\Delta\tilde{\eta}) = \frac{\tilde{p}(\Delta\tilde{\eta})}{p(\Delta\tilde{\eta})} \tag{79}$$

with the likelihood ratio for the k^{th} simulated path given by the product of these increments. The unbiased estimator is then

$$\hat{P}_{\mathrm{IS}} = \frac{1}{N}\sum_{k=1}^{N} I(\tilde{X}_{t_{\mathrm{f}}}^{(k)})l^{(k)}, \quad \text{with} \quad l^{k} = \prod_{j} l(\Delta\tilde{\eta}_j^{(k)}) \tag{80}$$

and with variance

$$\tilde{\mathbb{V}}\left[\hat{P}_{\mathrm{IS}}\right] = \frac{\tilde{\mathbb{E}}\left[I(\tilde{X}_{t_{\mathrm{f}}})l^2\right] - P^2}{N} \approx \frac{\mathbb{E}\left[I(\tilde{X}_{t_{\mathrm{f}}})l\right]}{N}, \tag{81}$$

where $\tilde{\mathbb{E}}$ and $\tilde{\mathbb{V}}$ denote expectation and variance with respect to the biased noise process.

A "good" importance sampling density is one that produces a small variance, i.e., one that satisfies $\tilde{p} \gg p$ for the events of interest, $x(t_{\mathrm{f}}) \notin \Omega$. In the present example, the biased density is determined by the control term in (77). In general, determining the control is a difficult task and one that depends sensitively on the deterministic dynamics and noise covariance structure. To motivate a particularly effective choice of b, we appeal again to the optimal control problem described above arising in the theory of large deviations. In particular, note that (77) essentially just adds noise to (43) with control $b = \sigma^{\dagger}\lambda$. Thus, building a control that satisfies (44) provides paths that form the most likely routes to the rare events of interest in (1).

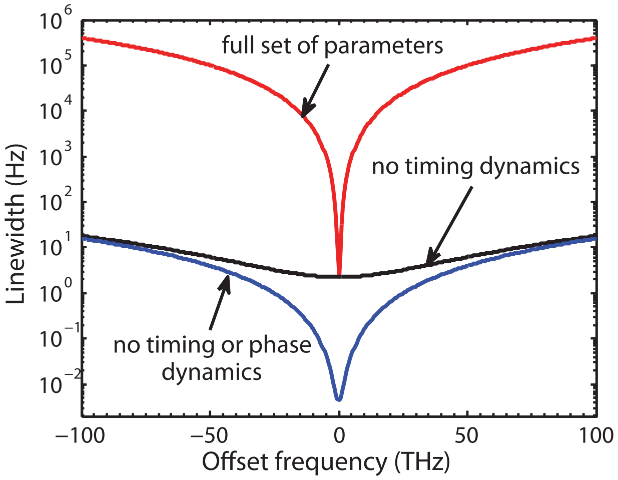

FIG. 6. *Linewidth analysis of a mode-locked laser, demonstrating the dominant role played by timing and phase dynamics in determining linewidth. Reproduced from Ref. [9].*

3. Applications.

3.1. Phase slips in mode-locked lasers. Mode-locked lasers provide an important example of systems subject to failure caused by large noise-induced phase excursions. These lasers produce pulses of light whose electric field envelope's phase is locked to the phase of the underlying carrier wave. In frequency space, this corresponds to a highly regular comb of laser lines with broad bandwidth and narrow linewidth [51]. Important applications of the temporal and spectral properties of mode-locked lasers depicted in Fig. (7) include laser manipulation of ultrafast chemical reactions and extremely precise measurement of time intervals [89].

A typical analysis of the effect of noise on laser operation is restricted to the induced linewidth obtained by linearizing the model equations for the laser about their desired operational state to produce Ornstein-Uhlenbeck dynamics; see for example [9],

$$\dot{x} = -Ax + \eta, \quad x = (\Delta g, \Delta w, \Delta\omega, \Delta\tau, \Delta\theta)^\dagger,$$

where Δg, Δw, $\Delta\omega$, $\Delta\tau$, and $\Delta\theta$ represent fluctuations in saturated gain, pulse energy, central frequency, central pulse timing, and phase, respectively. The conclusion suggested by Fig. 6 is that the timing and phase dynamics provide the dominant mechanisms by which noise affects linewidth. As explained below, however, this analysis neglects another important source of uncertainty.

The generation of a frequency comb with narrow individual lines over a broad spectral region requires precise control over the carrier-envelope phase offset, depicted as $\Delta\phi$ in Fig. 7. This control is implemented through interferometric feedback that typically only measures $\Delta\phi$ modulo full rotations of 2π. If a sequence of noise events successfully pushes $\Delta\phi$ to $\pm\pi$ (assuming without loss of generality that $\Delta\phi = 0$ for the noise-free operational state) then the feedback drives $\Delta\phi$ to the neighboring equilibrium value of $\pm 2\pi$. This situation is referred to as a phase slip and is an additional source of uncertainty in the laser's output. A noise-driven damped pendulum provides a good conceptual framework for these two sources of uncertainty, where

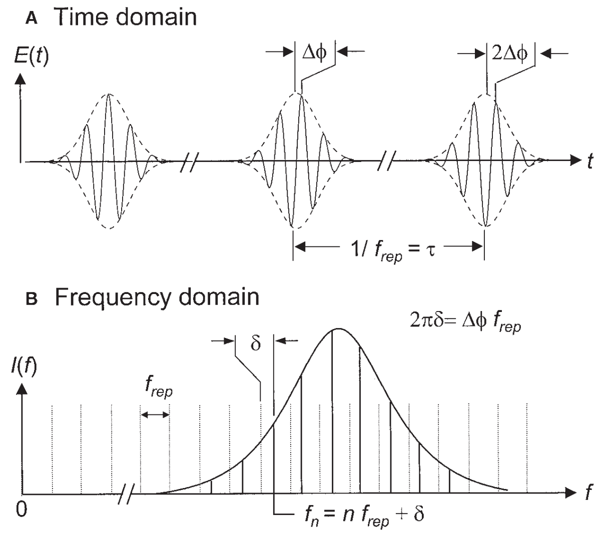

Fig. 7. *Sketch of electric field output from a mode-locked laser, in time (top) and in frequency space (bottom). A phase slip occurs when* $\Delta\phi$ *undergoes a noise-driven rotation of* 2π*. Reproduced from Ref. [51].*

the linewidth is provided by the stationary measure obtained in the small-amplitude limit of a damped linear oscillator, while phase slips correspond to the occasional full rotations induced in the pendulum by very unlikely sequences of noise increments.

To account for these rare events, consider the heuristic mode-locked laser model with active modulation introduced in Ref. [22]:

$$i\frac{\partial u}{\partial t}+\frac{1}{2}\frac{\partial^2 u}{\partial \xi^2}+|u|^2u=-c_0\cos(\omega\xi)u-ic_1u+ic_2\frac{\partial^2 u}{\partial \xi^2}+id_1|u|^2u-id_2|u|^4u+i\eta(\xi,t), \tag{82}$$

where u is the normalized complex electric field envelope, ξ is the averaged transverse variable (e.g., time, for temporal pulses as seen on an oscilloscope), and t is the longitudinal variable (e.g., a continuous approximation of the cavity round-trip index). Constants c_1, c_2, d_1, and d_2 respectively represent coefficients of linear cavity loss, spectral filtering, nonlinear gain, and gain saturation. Constants c_0 and ω are the amplitude and inverse width of active modulation intended to stabilize the pulse with its center position at the origin, and $\eta(\xi,t)$ is space-time white noise, with

$$\mathbb{E}[\eta^\dagger(\xi,t)\eta(\xi',t')]=D\delta(\xi-\xi')\delta(t-t'). \tag{83}$$

The stabilization term in (82) provides a restoring force on the pulse parameters that mitigates the impact of disturbances, including noise. This effect is characterized below through a linearized analysis of the reduced system of pulse parameters. The stabilization has a secondary effect, however, of producing additional equilibria that become dynamically accessible upon the introduction of noise. Transitions to these equilibria represent phase slips in the context of mode-locked lasers, and their rate of occurrence is an important quantity. We demonstrate below how this rate is computed approximately using the quasi-potential, and how the optimal paths provide insight into how phase slips arise.

When all coefficients are trivial, so that $c_0=c_1=c_2=d_1=d_2=D=0$, (82) is the integrable nonlinear Schrödinger equation, which supports a four-parameter

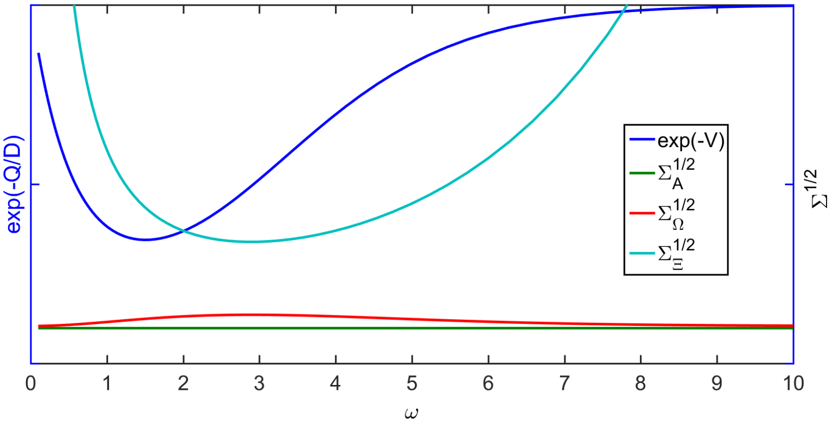

FIG. 8. *Left axis: Expected phase slip rate according to large deviation theory. Right axis: Square root of diagonal elements of covariance Σ, representing the root-mean-squared linewidth based on a conventional linearized analysis. Minimum escape probability is achieved at a different value of ω than minimum position jitter $\Sigma_\Xi^{1/2}$.*

family of soliton solutions with functional form

$$u_s(\xi,t) = A(t)\text{sech}\left[A(t)(\xi - \Xi(t))\right]e^{i\Theta(t)+i\xi\Omega(t)}, \tag{84}$$

where $\dot{A} = \dot{\Omega} = 0$, $\dot{\Xi} = \Omega$, and $\dot{\Theta} = \frac{1}{2}(A^2 - \Omega^2)$. In the perturbative limit where the coefficients are small, the dynamics of (82) can be approximated well for short times by a diffusion process in the four parameters induced by the noise term η [50]. Related approximations made outside of the perturbative limit are not rigorously justifiable yet often agree well with numerics [56]. We employ an approach based on averaging the Lagrangian density

$$L[u_s, u_{s\xi}, u_{st}] := \Im(u_{st}^* u_s) - \frac{1}{2}|u_{s\xi}|^2 + \frac{1}{2}|u_s|^4 + c_0\cos(\omega\xi)|u_s|^2. \tag{85}$$

of the variational (i.e., non-dissipative) terms in (82) over the ansatz expressed by (83). The dissipative terms in (82) are included through their projections against the tangent space of (83) [3, 8], i.e.,

$$\begin{aligned} &\nabla_y\mathcal{L} - \frac{\partial}{\partial t}\left(\nabla_{\dot{y}}\mathcal{L}\right) = \\ &\qquad 2\,\text{Re}\int i[-c_1u_s + c_2u_{s\xi\xi} + d_1|u_s|^2u_s - d_2|u_s|^4u_s + \eta(\xi,t)]\nabla_y u_s^*\,d\xi \end{aligned} \tag{86}$$

where $\mathcal{L} = \int L\,d\xi$ and $y = (A,\Omega,\Xi,\Theta)^T$. Note that this Lagrangian $\mathcal{L}$ and its density L are associated with the variational model reduction technique used in this application, and are not related to the Lagrangian associated with the action minimization described in Sec. 2.2.

Keeping only the first three components of y, i.e., $x_j = y_j$ for $j = 1,\ldots,3$, we have

$$\dot{x} = f(x) + \sigma(x)\eta(t) \tag{87}$$

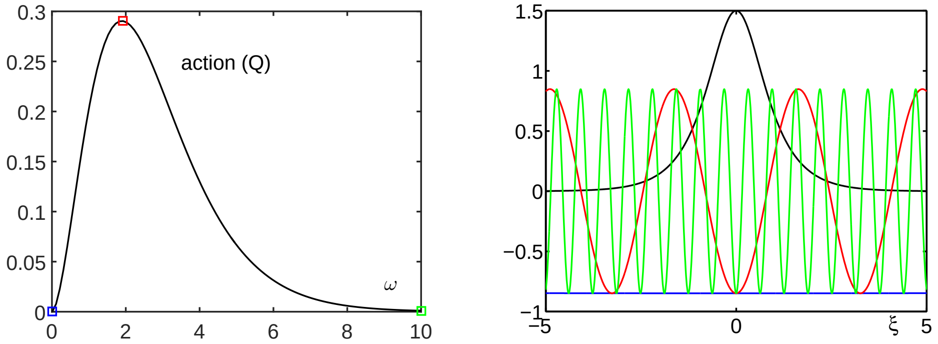

FIG. 9. *(a) Minimum action connecting stable fixed point at origin ($n = 0$) to saddle ($n = 1$), plotted vs. parameter ω from (82). (b) Laser pulse (black) and active feedback for $\omega = 0$ (blue), $\omega = 1.9$ (red), and $\omega = 10$ (green), corresponding to the squares in (a).*

with drift

$$f(x) = \begin{pmatrix} -2c_1x_1 + (\tfrac{4}{3}d_1 - \tfrac{2}{3}c_2)x_1^3 - \tfrac{16}{15}d_2x_1^5 - 2c_2x_1x_2^2 \\ -\tfrac{4}{3}c_2x_1^2x_2 - \pi c_0\omega^2 \operatorname{csch}(\pi\omega/2x_1)\sin(\omega x_3)/2x_1^3 \\ x_2 \end{pmatrix} \tag{88}$$

and diffusivity

$$\sigma(x) = \begin{pmatrix} \sqrt{x_1} & 0 & 0 \\ 0 & \sqrt{x_1/3} & 0 \\ -x_3/\sqrt{x_1} & 0 & \sqrt{\pi^2/12x_1^3 + x_3^2/x_1} \end{pmatrix}. \tag{89}$$

The phase dynamics for $y_4 = \Theta$ are slaved to the other independent variables, with

$$\begin{aligned} \dot{\Theta} = & -\frac{\pi\omega c_0}{A^3}\cos(\omega\Xi)\operatorname{csch}\left(\frac{\pi\omega}{2A}\right)\left(1 + \frac{\pi\omega}{2A^2}\coth\left(\frac{\pi\omega}{2A}\right)\right) \\ & - \Xi + \frac{1}{2}(A^2 - \Omega^2) + \left(\frac{\sqrt{12+\pi^2}}{6\sqrt{A}}\right)\eta_4. \end{aligned} \tag{90}$$

The noise term $\eta(t) \in \mathbb{R}^3$ in (87) satisfies

$$\mathbb{E}[\eta(t)\eta(t')^T] = DI\delta(t - t') \tag{91}$$

and is obtained from $\eta(\xi, t)$ in (82) using the same averaged Lagrangian method, and essentially represents that portion of the stochastic driving term that directly influences the parameters in x. Matrix I is the 3×3 identity.

In the deterministic ($D = 0$) limit, the nontrivial equilibria are $x^{(n)} = (A_0,\ 0,\ n\pi/\omega)$ for $n \in \mathbb{Z}$, with

$$A_{0\pm}^2 = \frac{5}{16d_2}\left(2d_1 - c_2 \pm \sqrt{(2d_1 - c_2)^2 - \frac{96}{5}c_1d_2}\right).$$

Of these, the equilibria with A_{0+} are stable nodes or spirals for n even and saddles for n odd. The equilibria with A_{0-} are always saddles. To repeat the analysis from Ref. [9], linearization about u_0 gives steady state covariance

$$\Sigma = \frac{D}{2\pi}\int ds\,\left[(isI - M)^{-1}\sigma(x^0)\right]\left[(isI - M)^{-1}\sigma(x^0)\right]^{\dagger}, \tag{92}$$

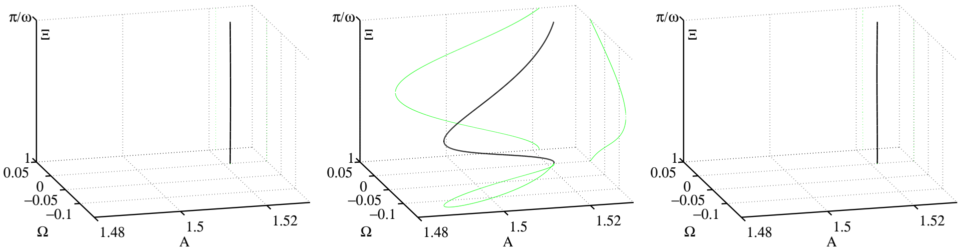

FIG. 10. *Minimum action paths from stable fixed point ($n = 0$) to saddle ($n = 1$) for (a) $\omega = 0$, (b) $\omega = 1.9$, and (c) $\omega = 10$, corresponding to squares in Fig. 9(a).*

where

$$M = \begin{pmatrix} 8c_1 - \frac{4}{3}(2d_1 - c_2)A_0^2 & 0 & 0 \\ 0 & -\frac{4}{3}c_2 A_0^2 & -\frac{(-1)^n \pi c_0 \omega^3}{2A_0^3}\operatorname{csch}(\frac{\pi\omega}{2A_0}) \\ 0 & 1 & 0 \end{pmatrix}. \tag{93}$$

As discussed above, however, the feedback mechanism requires that we consider two sources of uncertainty in the laser output, the first associated with laser linewidth and the second associated with the expected rate of phase slips. A complete analysis of the phase slip rate requires a consideration of the phase dynamics expressed by (87) and (90), including contributions from the dynamics of all other parameters. For simplicity of presentation, we consider here transitions between the equilibria described above, noting that the drift term in (90) changes by $2\pi/\omega$ between neighboring stable equilibria. In appropriate parameter regimes, this is the dominant contributing factor to phase slips.

As described in Sec. 2.3, the expected time for transition between neighboring equilibria is $\exp(Q(x^0, x^2)/D)$, where Q is the quasi-potential. Figure 8 plots these distinct types of uncertainty against one of the active feedback parameters, ω, where the reciprocal of the transition time has been expressed as a rate. It is clear from the figure that one cannot in general expect to be able to minimize both linewidth and phase slip rate simultaneously; practical considerations inform the balance that must be struck between these sources of uncertainty [66].

Although the action Q provided by the GMAM computation is the quantity that determines the mean exit rate estimate, it is also instructive to examine the paths associated with minimum action for various choices of physical constants.

Figure 9 graphs the minimum action as a function of the inverse width of the active feedback trap, represented by ω in (82). For small values of ω, the trap is so wide as to be essentially constant over the support of the pulse. This leaves (82) effectively invariant with respect to translations of the pulse offering no restoring force to noise that moves the pulse's position from the origin. The action for a change in position along this neutrally stable manifold is therefore zero. This is reflected in Fig. 10(a), where the most likely transition path involves simple translation in ξ. Conversely, for large values of ω, as seen in the green curve, the trap's wavelength is much shorter than the pulse's width, so that its ability to stop the pulse from moving is limited. Neighboring equilibria are also very close together in this limit. The action therefore approaches zero and the most likely transition path between equilibria is again a linear translation, as shown in Fig. 10(c). Between these values of ω, however, is a range of values where variations of the trap are commensurate in scale with the support of the soliton, such that the trap offers maximal resistance to large excursions and generates a large value of action. Figure 10(b) shows that this increased action is associated with an exit path that exploits the internal dynamics of the SDE much more significantly. This picture is qualitatively similar to the impact of varying ω on the standard deviation, or jitter, in pulse position, but the minimum is achieved at a different value of ω, as illustrated in Fig. 8.

Figure 11 illustrates a different dependence of action on parameter value c_0, the amplitude of the active feedback trap for fixed $\omega = 1$. In this case, the action increases monotonically with c_0, and the minimum action paths are seen to become more and more tortuous as the trap becomes more and more effective at blocking the transition mechanism of simple translation.

3.2. Importance sampling for large soliton walks. In the laser dynamics example in Sec. 3.1, the minimum action calculated for passage from a stable fixed point to a neighboring saddle is used to approximate the average rate at which noise is expected to drive the laser from its desired operating point. The paths associated with these minimum action computations are informative in their own right since they illustrate the dynamic paths taken on these most probable excursions. In fact, these paths provide the information necessary to implement importance sampling in Monte Carlo simulations designed to compute correct expectations of exit probabilities in finite time as described in Sec. 2.6. Figure 12 demonstrates that these paths change significantly as the time horizon for an exit is varied, from a geodesic path with respect to a norm dictated by the diffusion tensor to the limiting path corresponding to the quasi-potential calculations from Sec. 3.1.

For exit probabilities on finite times, traditional large deviation theory provides

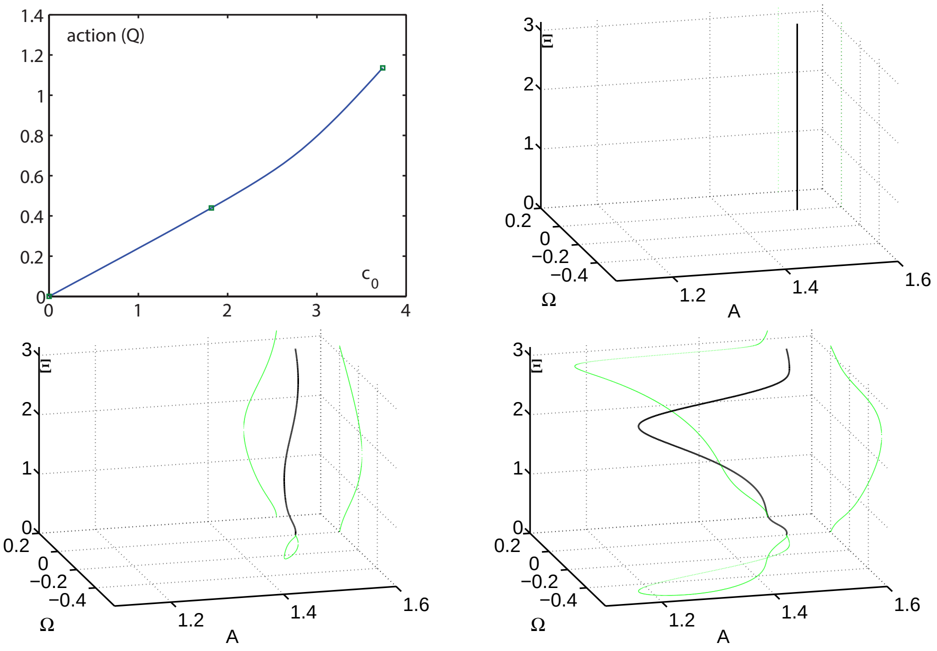

Fig. 11. *(a) Minimum action path connecting stable fixed point at origin ($n = 0$) to saddle ($n = 1$), plotted vs. parameter c_0 from (82). Minimum action paths for squares on (a) are plotted in (b), (c), and (d).*

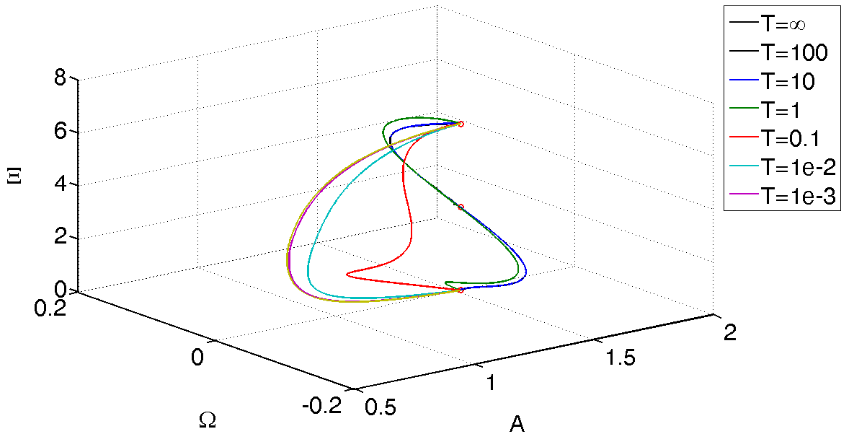

FIG. 12. *Minimum action paths for the SDE given by (87) as the horizon time* t_{f} *is varied.*

an asymptotic scaling law,

$$\lim_{D\to 0} D \ln P\left(x(t_{\mathrm{f}}) \notin \Omega\right) = -\inf_{x(t_{\mathrm{f}})\notin\Omega} \mathcal{S}_{t_{\mathrm{f}}}[x], \tag{94}$$

where the probability P contains an undetermined prefactor. For the reduced model provided by (87), computing this prefactor is at least possible using more substantial analysis of the Fokker-Planck equation [63]. Given that the model reduction from the stochastic PDE (82) is itself imperfect, one would ideally seek to perform Monte Carlo simulations on the original model to verify the accuracy of estimates obtained through the reduced model. To compute exit probabilities in the context of small noise, a naive Monte Carlo approach is computationally prohibitive, requiring the use of importance-sampled Monte Carlo simulations based on the paths computed above [67, 68, 83].

For example, a simplified version of (82) relevant to optical communications includes spectral filtering, compensatory gain ($c_1 < 0$), and white noise:

$$i\frac{\partial u}{\partial t}+\frac{1}{2}\frac{\partial^2 u}{\partial \xi^2}+|u|^2 u = -ic_1 u + ic_2\frac{\partial^2 u}{\partial \xi^2} + i\eta(\xi,t). \tag{95}$$

Filters have been used as a mechanism for reducing jitter in the position of solitons by adding a restoring force to the spatial frequency, which is tied to the soliton's speed through the dispersion relation [50]. Damping fluctuations in spatial frequency is therefore an effective way to suppress position jitter, as illustrated in Fig. 13. The same reduction method used above produces the SDE given by

$$\dot{x} = f(x) + \sigma(x)\eta \tag{96}$$

with $x = (A,\, \Omega,\, \Xi)^T$, where the drift is

$$f(x) = \begin{pmatrix} -2c_1x_1 - \frac{2}{3}c_2x_1^3 - 2c_2x_1x_2^2 \\ -\frac{4}{3}c_2x_1^2x_2 \\ x_2 \end{pmatrix}, \tag{97}$$

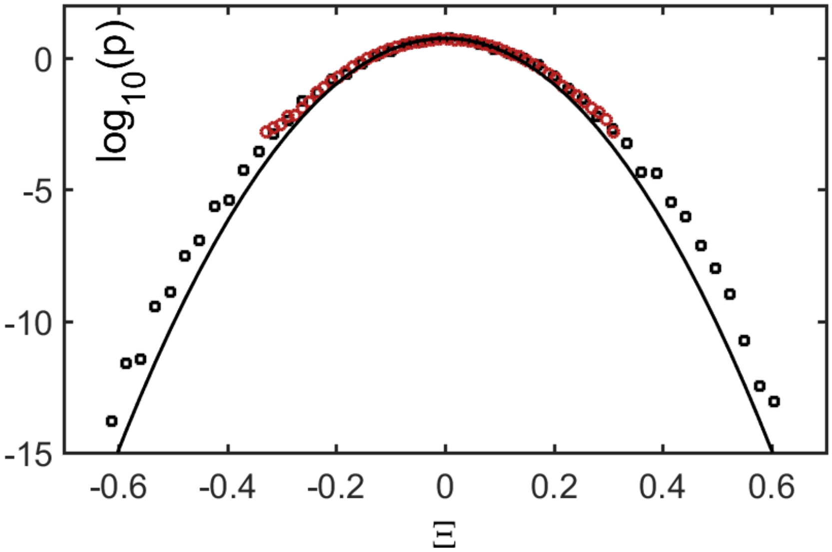

Fig. 13. *Probability density p associated with the diffusion of position Ξ obtained from importance-sampled Monte Carlo simulations of the stochastic PDE (95) (black squares) and from unbiased simulations (brown circles). The black curve is the Gaussian probability density function predicted by linearizing the reduced ODE given by (96)-(98).*

and diffusivity is

$$\sigma(x) = \begin{pmatrix} \sqrt{x_1} & 0 & 0 \\ 0 & \sqrt{x_1/3} & 0 \\ -x_3/\sqrt{x_1} & 0 & \sqrt{\pi^2/12x_1^3 + x_3^2/x_1} \end{pmatrix}, \tag{98}$$

and where we have again omitted the dynamics in Θ. The GMAM method presented in Sec. 2.3 can be applied to compute the optimal path from a pulse centered at the origin with amplitude, frequency, and position coordinates $(A, \Omega, \Xi) = (1, 0, 0)$ to a final position $\Xi(t_\mathrm{f}) = \Xi_f$ with the other two final coordinates left unspecified. By picking different values of Ξ_f, one can reconstruct a histogram of probabilities from which the entire probability density function (pdf) for the final position Ξ can be computed well down into the low-probability tails. Figure 13 illustrates such a reconstructed pdf, where 50,000 importance-sampled Monte Carlo simulations of the stochastic PDE (95) have been used to compute pdf tail probabilities on the order of 10^{-12} and below. Also shown is the Gaussian pdf predicted by a linearization of the ODE reduction given by (96)-(98). This curve and simulations of the nonlinear ODEs (not shown) demonstrate that the low-order reduction fails to accurately compute probabilities in the tails of the pdf, but Fig. 13 clearly shows that it is effective at generating appropriately biased simulations of the original PDE model.

3.3. Extinction in biological populations. We now consider internal noise and how it may induce the rare event of extinction of a species or of an infectious disease. Extinction can be good (disease) or bad (species); either way, it is important to understand why and how often it can be expected to happen for different model parameters. We consider two examples: (1) the Susceptible-Infectious-Susceptible (SIS) epidemic model, and (2) the Allee effect model.

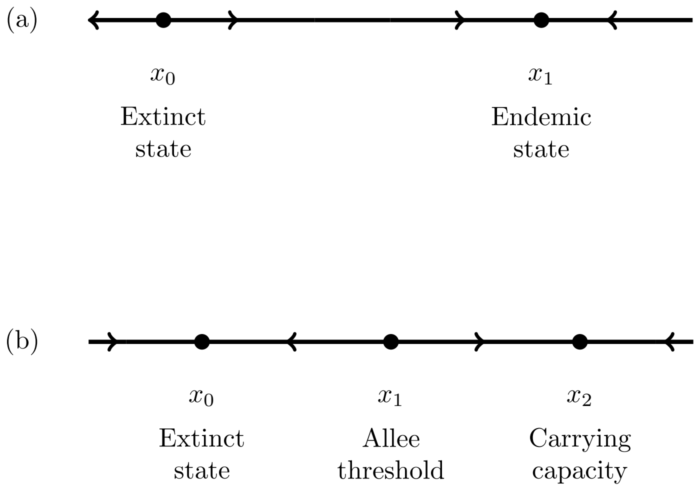

FIG. 14. *(a) Topology of the deterministic SIS model. There are two fixed points: a stable endemic state and an unstable extinct state. (b) Topology of the deterministic Allee effect model. There are three fixed points: a stable carrying capacity, a stable extinct state, and an unstable Allee threshold.*

The deterministic SIS model has two fixed points. One is an extinct state where no infectious individuals are present, while the other is an endemic state where the infection is maintained. The stability of these two fixed points is determined by the value of the reproductive number R_0. The reproductive number can be thought of as the average number of new infectious individuals that one infectious individual generates over the course of the infectious period, in an entirely susceptible population. For $R_0 > 1$, the extinct state is unstable while the endemic state is stable, as shown in Fig. 14(a). Note that since the model is deterministic, a population at the attracting endemic state can never go extinct.

The deterministic Allee effect model has three fixed points. One can see in Fig. 14(b) that the extinct state x_0 is stable, as is the carrying capacity x_2. The Allee threshold x_1 is unstable, so when initial values lie between x_1 and x_2, the deterministic solution will increase to x_2, while for initial values less than x_1 the deterministic solution decreases to the extinct state. Similar to the deterministic SIS, a population at the attracting carrying capacity can never go extinct.

To capture extinction events, we must consider a stochastic model with internal noise that represents the random interactions of individuals in the population. Figure 15 shows a time series of infectious individuals for a stochastic SIS model. One can see fluctuations about the endemic state for a long period of time until eventually the noise-induced rare event (extinction) occurs. Similarly, Fig. 2 shows a time series of individuals for a stochastic Allee effect model. One sees the population fluctuating about the carrying capacity for a long period of time until the rare extinction event occurs. Details of the Monte Carlo method used in both simulations can be found in Appendix A.

The two examples considered in this section have different mean-field topologies as seen in Fig. 14. For the SIS model, the extinct state x_0 is a repelling point of the deterministic mean-field equation, while the endemic state x_1 is an attracting point. In this extinction scenario, the optimal path to extinction is a heteroclinic trajectory

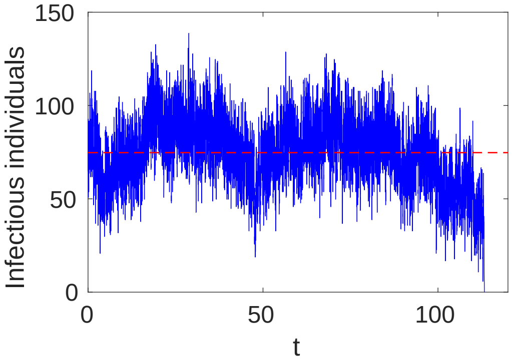

FIG. 15. *Stochastic realization of an SIS system showing extinction after fluctuating about the endemic state for a long time.*

with non-zero momentum that connects the equilibrium point $(x, \lambda) = (x_1, 0)$ with a fluctuational extinct state $(x, \lambda) = (0, \lambda_f)$. This new fluctuational extinct state is an equilibrium point of Hamilton's equations given by (69). Figure 16 shows the optimal path topology in the expanded 2D space.

For the Allee effect model, the extinct state x_0 is an attracting point of the deterministic mean-field equation. Additionally, there is an intermediate repelling point x_1 that lies between the extinct state and another attracting state x_2. In this extinction scenario, the optimal path to extinction, is composed of two segments. The first segment is a heteroclinic trajectory with non-zero momentum that connects the equilibrium point $(x, \lambda) = (x_2, 0)$, with the intermediate equilibrium point $(x, \lambda) = (x_1, 0)$. The second segment consists of the segment along $\lambda = 0$ from x_1 to the extinct state x_0. Figure 17 shows the optimal path topology in the expanded 2D space.

3.3.1. SIS epidemic model. The SIS problem has mean-field equations given as

$$\dot{S} = \mu K - \frac{\beta}{K} SI + \gamma I - \mu S, \tag{99a}$$

$$\dot{I} = \frac{\beta}{K} SI - \gamma I - \mu I, \tag{99b}$$

where β is the contact rate, γ is the recovery rate, and μ is the birth/death rate. Using a constant population assumption $S + I = K$ leads to [59, 69, 4, 70]

$$\dot{I} = \frac{\beta}{K}(K - I)I - \gamma I - \mu I. \tag{100}$$

Steady states of (100) are $I = 0$, and $I = K\left(1 - \frac{1}{R_0}\right)$, where $R_0 = \frac{\beta}{\mu+\gamma}$ is the reproductive number. The endemic state is stable for $R_0 > 1$, as seen in Fig. 14(a). Therefore, deterministically, there is no way for the disease to go extinct as mentioned previously. However, as shown in Fig. 15, the internal noise can in fact induce a large fluctuation which brings the population into the extinct state. Employing the theory described in Secs. 2.4 and 2.5, one can find the optimal path to extinction which connects the deterministic endemic state to a new fluctuational extinct state.

We constrain the population size so that $S = K - I$. This allows one to consider the dynamics of the constrained SIS model in terms of only the infectious individuals

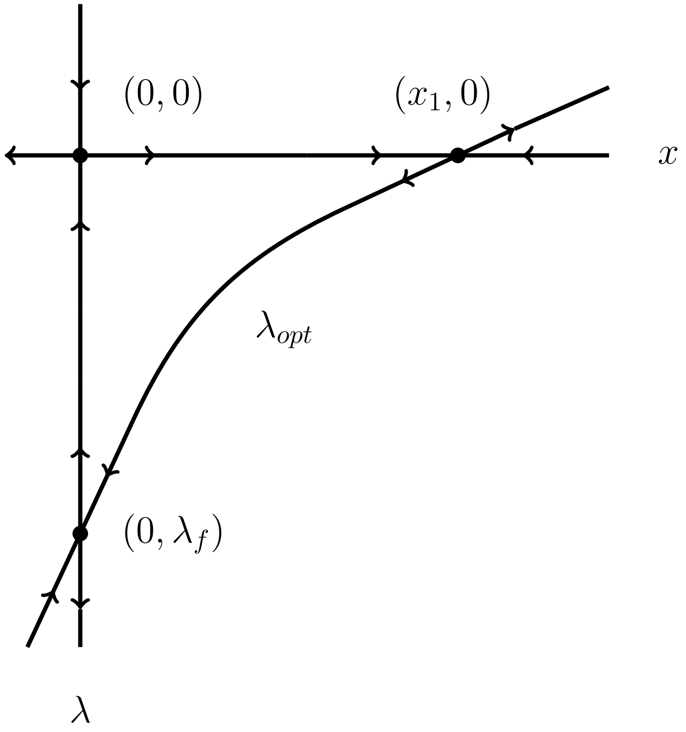

Fig. 16. *Steady states of Hamilton's equations (69) and zero-energy trajectories of the Hamiltonian (68) for the SIS model as well as other models with deterministic mean-field topology of the type shown in 14(a). The extinct state $x_0 = 0$ is a repelling point of the deterministic mean-field equation, while the endemic state x_1 is an attracting point. In this extinction scenario, the optimal path to extinction λ_{opt} is a heteroclinic trajectory with non-zero momentum that connects the equilibrium point $(x,\lambda) = (x_1, 0)$ with a fluctuational extinct state $(x,\lambda) = (0,\lambda_f)$.*

I. Rescaling time by $\mu+\gamma$, the mean-field equation of the constrained SIS model becomes

$$\dot{I} = \frac{R_0}{K}(K-I)I - I. \tag{101}$$

In rescaling time by $\mu+\gamma$, the corresponding stochastic population model is represented by the transition processes of infection, and removal due to recovery [21, 26, 79]. The associated rates $W(X;r)$ are given as

Infection:	$W(I;1) = (R_0/K)I(K-I)$
Recovery:	$W(I;-1) = I$

and the master equation is then

$$\frac{\partial \rho(I,t)}{\partial t} = [(I+1)\rho(I+1,t) - I\rho(I,t)] \tag{102}$$

$$+ \frac{R_0}{K}[(I-1)(K-(I-1))\rho(I-1,t) - I(K-I)\rho(I,t)]. \tag{103}$$

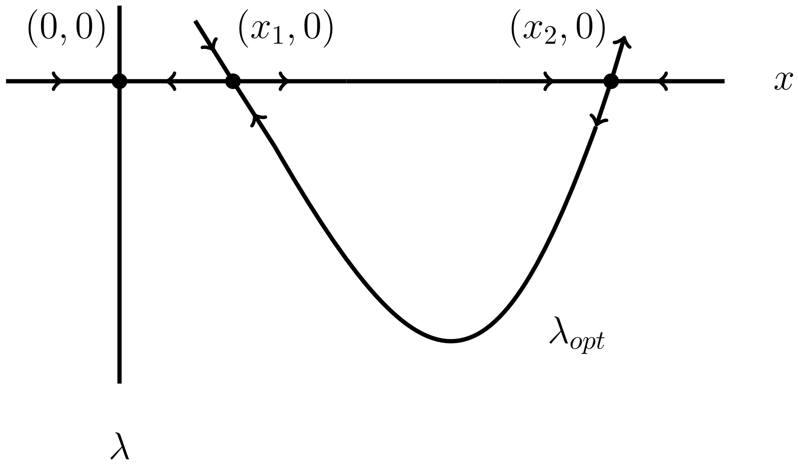

FIG. 17. *Steady states of Hamilton's equations (69) and zero-energy trajectories of the Hamiltonian (68) for the Allee effect model as well as other models with deterministic mean-field topology of the type shown in 14(b). The extinct state $x_0 = 0$ is an attracting point of the deterministic mean-field equation. Additionally, there is an intermediate repelling point x_1 that lies between the extinct state and another attracting state x_2. In this extinction scenario, the optimal path to extinction, is composed of two segments. The first segment is a heteroclinic trajectory with non-zero momentum that connects the equilibrium point $(x, \lambda) = (x_2, 0)$, with the intermediate equilibrium point $(x, \lambda) = (x_1, 0)$. The second segment consists of the segment along $\lambda = 0$ from x_1 to the extinct state x_0.*

The scaled transition rates in (64) are given as

$$\begin{aligned} w_{+1}(x) &= R_0(1-i)i, & w_{-1}(x) &= i, \\ u_{+1}(x) &= 0, & u_{-1}(x) &= 0, \end{aligned} \tag{104}$$

where $i = I/K$ is the fraction of infectious individuals in the population.

Substitution of (104) into (68) leads to the Hamiltonian given as

$$\mathcal{H}(I, \lambda) = R_0(1-i)i(e^{\lambda} - 1) + i(e^{-\lambda} - 1). \tag{105}$$

Solutions to $\mathcal{H}(I, \lambda) = 0$ are

$$i = 0, \quad \lambda = 0, \quad \text{and} \quad \lambda(i) = -\ln\left(R_0(1-i)\right). \tag{106}$$

The third solution is λ_{opt} and can also be found using (71). Taking derivatives of (105) with respect to x and λ (see (69)) leads to the following system of Hamilton's equations:

$$\dot{i} = \frac{\partial \mathcal{H}}{\partial \lambda} = R_0(1-i)ie^{\lambda} - ie^{-\lambda}, \tag{107a}$$

$$\dot{\lambda} = -\frac{\partial \mathcal{H}}{\partial i} = -R_0(1-2i)(e^{\lambda} - 1) - (e^{-\lambda} - 1). \tag{107b}$$

This system of Hamilton's equations has three steady states given by an extinct state $(i, \lambda) = (0, 0)$, an endemic state $(i, \lambda) = (1 - 1/R_0, 0)$, and a fluctuational extinct state $(i, \lambda) = (0, -\ln(R_0))$. These steady states along with the zero energy curves of the Hamiltonian are shown in Fig. 18.

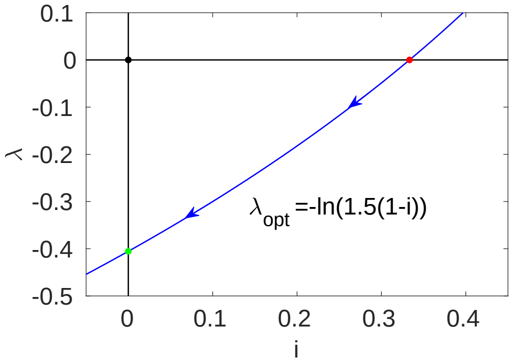

FIG. 18. *Steady states of Hamilton's equations (107) and zero-energy curves of the SIS model Hamiltonian (105) for* $R_0 = 1.5$. *The extinct state is located at* $(0, 0)$ *(black dot), the endemic state is located at* $(1/3, 0)$ *(red dot), and the fluctuational extinct state is located at* $(0, -\ln(1.5))$ *(green dot). The optimal path* $\lambda_{opt} = -\ln(1.5(1-i))$ *(blue curve) runs from the endemic state to the fluctuational extinct state.*

The action along the optimal path given by (72) is

$$\mathcal{S}_{\text{opt}} = \int_{1-\frac{1}{R_0}}^{0} \lambda(i)\, di = \ln(R_0) - 1 + \frac{1}{R_0}. \tag{108}$$

The general form of the MTE for single-step problems with a similar topology to that shown in Fig. 14(a) is

$$\tau = \frac{\sqrt{2\pi R}\exp\left(\int_{x_0}^{x_1}\left(\frac{u_{+1}(x)}{w_{+1}(x)} - \frac{u_{-1}(x)}{w_{-1}(x)}\right)dx\right)}{(R-1)w_{+1}(x_1)\sqrt{K\lambda'_{opt}(x_1)}} \exp\left(K\int_{x_0}^{x_1}\ln\left(\frac{w_{+1}(x)}{w_{-1}(x)}\right)dx\right), \tag{109}$$

where $R = w'_{+1}(0)/w'_{-1}(0)$. The SIS problem therefore has a MTE given as

$$\tau = B\exp(K\mathcal{S}_{\text{opt}}) = \frac{R_0}{(R_0-1)^2}\sqrt{\frac{2\pi}{N}}\exp\left[K\left(\ln(R_0) - 1 + \frac{1}{R_0}\right)\right]. \tag{110}$$

The analytical MTE is confirmed using numerical simulations. By numerically computing thousands of stochastic realizations and the associated extinction times, one can calculate the MTE. Figure 19 shows a comparison of the analytical and numerical mean time to extinction as a function of reproductive number R_0. There is excellent agreement except at low R_0 where the quasi-stationary assumption breaks down.

3.3.2. Allee effect model. The Allee effect problem has a mean-field equation given as

$$\dot{x} = \frac{\alpha x^2}{2} - \mu x - \frac{\sigma x^3}{6}, \tag{111}$$

where μ is the death rate of low-density populations, α is the growth rate when the population is large enough, and σ is a negative growth rate for an overcrowded population.

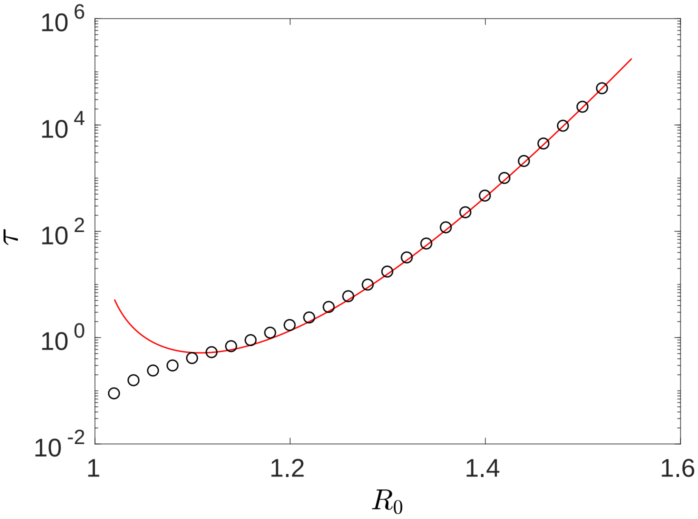

Fig. 19. *Comparison of analytical (red curve) and numerical (black circles) mean time to extinction versus* R_0 *for SIS model.*

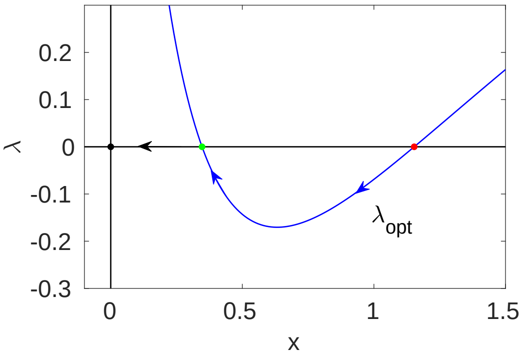

Fig. 20. *Steady states of Hamilton's equations (115) and zero-energy curves of the Hamiltonian (113) for* $\mu = 0.2$, $\alpha = 1.5$, *and* $\sigma = 3$. *The extinct state is located at* $(0, 0)$ *(black dot), the Allee threshold state is located at* $(0.35, 0)$ *(green dot), and the carrying capacity state is located at* $(1.15, 0)$ *(red dot). The optimal path* $\lambda_{opt} = -\ln\left[(1.2 + 3x^2)/4.5x\right]$ *(blue curve) runs from the carrying capacity state to the Allee threshold state, and from there continues deterministically to the extinct state.*

The steady states of (111) are $x_0 = 0$, and $x_{1,2} = \frac{3\alpha\mp\sqrt{9\alpha^2-24\sigma\mu}}{2\sigma}$, where x_0 is stable, x_1 is unstable, and x_2 is stable as shown in Fig. 14(b) [6, 71]. Therefore, deterministically, there is no way for the disease to go extinct, as mentioned previously. However, as shown in Fig. 2 the internal noise can in fact induce a large fluctuation which brings the population to a vicinity of the repelling fixed point of the deterministic rate equation. From there, the population travels essentially deterministically to the extinct state. Employing the theory described in Secs. 2.4 and 2.5, one can find the optimal path to extinction.

The corresponding stochastic population model is represented by the following transition processes and associated rates $W(X;r)$.

$$\begin{aligned} &X \xrightarrow{\mu} \varnothing && \mu X, \\ &2X \xrightarrow{\alpha/K} 3X && \alpha\tfrac{X(X-1)}{2K}, \\ &3X \xrightarrow{\sigma/K^2} 2X && \sigma\tfrac{X(X-1)(X-2)}{6K^2}. \end{aligned}$$

The first two transitions involving the death rate μ and the growth rate α are required to capture the Allee effect. The negative growth rate σ allows for an overcrowded population to decline to the carrying capacity K [6, 71].

The scaled transition rates in (64) are given as

$$\begin{aligned} w_{+1}(x) &= \tfrac{\alpha x^2}{2}, & w_{-1}(x) &= \mu x + \tfrac{\sigma x^3}{6}, \\ u_{+1}(x) &= -\tfrac{\alpha x}{2}, & u_{-1}(x) &= -\tfrac{\sigma x^2}{2}. \end{aligned} \tag{112}$$

Substitution of (112) into (68) leads to the Hamiltonian given as

$$\mathcal{H}(x,\lambda) = \frac{\alpha x^2}{2}(e^{\lambda}-1) + \left(\mu x + \frac{\sigma x^3}{6}\right)(e^{-\lambda}-1). \tag{113}$$

Solutions to $\mathcal{H}(x,\lambda)=0$ are

$$x = 0, \quad \lambda = 0, \quad \text{and} \quad \lambda(x) = \ln\left(\frac{6\mu + \sigma x^2}{3\alpha x}\right). \tag{114}$$

The third solution is λ_{opt} and can also be found using (71). Taking derivatives of (113) with respect to x and λ (see (69)) lead to the following system of Hamiltons equations:

$$\dot{x} = \frac{\partial \mathcal{H}}{\partial \lambda} = \frac{\alpha x^2}{2}e^{\lambda} - \left(\mu x + \frac{\sigma x^3}{6}\right)e^{-\lambda}, \tag{115}$$

$$\dot{\lambda} = -\frac{\partial \mathcal{H}}{\partial x} = -\alpha x(e^{\lambda}-1) - \left(\mu + \frac{\sigma x^2}{2}\right)(e^{-\lambda}-1). \tag{116}$$

This system of Hamilton's equations has three steady states given as $(x,\lambda) = (x_0,0) = (0,0)$, $(x,\lambda) = (x_1,0)$, and $(x,\lambda) = (x_2,0)$ where x_0, x_1, and x_2 are the steady states of the mean-field equation (111) provided above. These steady states along with the zero energy curves of the Hamiltonian are shown in Fig. 20.

The general form of the MTE for single-step problems with a similar topology to that shown in Fig. 14(b) is

$$\tau = \frac{2\pi \exp\left(\int_{x_1}^{x_2}\left(\frac{u_{+1}(x)}{w_{+1}(x)} - \frac{u_{-1}(x)}{w_{-1}(x)}\right)dx\right)}{w_1(x_2)\sqrt{|\lambda'_{opt}(x_1)|\lambda'_{opt}(x_2)}} \exp\left(K\int_{x_2}^{x_1}\ln\left(\frac{w_{-1}(x)}{w_{+1}(x)}\right)dx\right). \tag{117}$$

It is worth noting that the derivation of (117) involves matching the solution from x_2 to x_1 asymptotically with the deterministic solution from x_1 to x_0. Because this latter solution is associated with $\lambda = 0$, its final form does not involve an integral from x_1 to x_0. Nevertheless, the deterministic contribution is in fact included in (117).

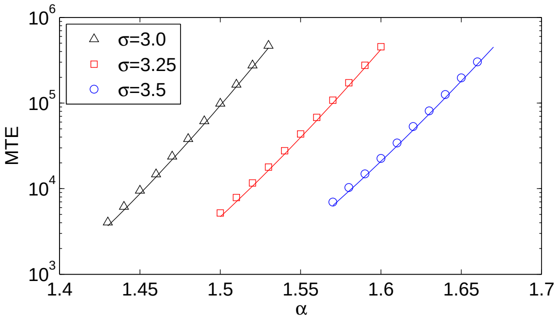

FIG. 21. *Comparison of analytical and numerical mean time to extinction versus α for various σ for the stochastic Allee effect problem.*

Details regarding the derivation of the prefactor B in (109) and (117) as well as details regarding the MTE for multi-step problems can be found in [6].

The analytical MTE for the Allee effect problem is found using (117) and is confirmed using numerical simulations. By numerically computing thousands of stochastic realizations and the associated extinction times, one can calculate the MTE. Figure 21 shows the comparison between the analytical and the numerical mean time to extinction as a function of α for various choices of σ [71].

4. Conclusions. The study of rare events in noise-driven physical and biological models presents a unique opportunity to combine tools from different arenas of applied mathematics, including variational calculus, optimal control, singular perturbation theory, WKBJ theory, asymptotics of integrals, and sampling techniques, to provide considerable insight into ostensibly intractable problems. The examples included here are just a sample of the important questions that can be answered by an intuitive combination of theory and numerics. The applicability of these tools can only grow with the explosion of interest in stochastic partial differential equations and geometric growth in computing power. It is the authors' hope that this primer facilitates the entry of new researchers into this exciting and rapidly growing field.

Appendix A. Numerical Methods for Stochastic Differential Equations.

The simplest numerical method to generate a random walk approximating a diffusion process is the stochastic Euler method, sometimes referred to as the Euler-Maruyama method. Given the Itô stochastic differential equation expressed in (5), the stochastic Euler scheme is given by

$$X_{n+1} = X_n + f(X_n)\Delta t + \sigma(X_n)\Delta\eta_n, \tag{118}$$

where the time increment is $\Delta t = t_{n+1} - t_n$ and the noise increment is $\Delta\eta_n = \eta_{t_{n+1}} - \eta_{t_n}$. To implement the stochastic Euler scheme, we note that the noise increments are independent Gaussian random variables with the following first and second moments:

$$\mathbb{E}(\Delta\eta_n) = 0, \qquad \mathbb{E}((\Delta\eta_n)^2) = D\Delta t, \tag{119}$$

so that

$$\Delta\eta_n \sim \mathcal{N}(0, D\Delta t). \tag{120}$$

In practice, one can solve (118) numerically, using a random number generator to draw noise values from the distribution given by (120). Alternatively, one can numerically solve

$$X_{n+1} = X_n + f(X_n)\Delta t + \sqrt{D\Delta t}\,\sigma(X_n)\,\hat{\eta}_n, \tag{121}$$

where

$$\hat{\eta}_n \sim \mathcal{N}(0,1). \tag{122}$$

For the Ornstein-Uhlenbeck process expressed by $f(x) = -x$ with $D\sigma \equiv 1$, this becomes

$$X_{n+1} = (1-\Delta t)X_n + \sqrt{\Delta t}\,\eta_n, \qquad \eta_n \sim \mathcal{N}(0,1). \tag{123}$$

To generate a solution of a stochastic equation, where the noise is internal, we use the Doob-Gillespie algorithm (also known as the Gillespie algorithm or Gillespie's stochastic simulation algorithm (SSA)) [23, 43]. The algorithm is a type of Monte Carlo method that was originally proposed by Kendall [53] for simulating birth-death processes and was popularized by Gillespie [43] as a useful method for simulating chemical reactions based on molecular collisions. The results of a Gillespie simulation is a stochastic trajectory that represents an exact sample from the probability function that solves the master equation. Therefore the method can be used to simulate population dynamics where molecular collisions are replaced by individual events and interactions including birth, death, and infection.

Let $\mathbf{x} = (x_1, \ldots, x_n)^T$ denote the state variables of a system, where x_i provides the number of individuals in state x_i at time t. The first step of the algorithm is to initialize the number of individuals in the population compartments $\mathbf{x}_0$. For a given state $\mathbf{x}$ of the system, one calculates the transition rates (birth rate, death rate, contact rate, etc.) denoted as $a_i(\mathbf{x})$ for $i = 1 \ldots l$, where l is the number of transitions. Thus the sum of all transition rates is given by $a_0 = \sum_{i=1}^{l} a_i(\mathbf{x})$.

Random numbers are generated to determine both the next event to occur as well as the time at which the next event will occur. One simulates the time τ until the next transition by drawing from an exponential distribution with mean $1/a_0$. This is equivalent to drawing a random number r_1 uniformly on $(0,1)$ and computing $\tau = (1/a_0)\ln(1/r_1)$. During each random time step exactly one event occurs. The probability of any particular event taking place is equal to its own transition rate divided by the sum of all transition rates $a_i(\mathbf{x})/a_0$. A second random number r_2 is drawn uniformly on $(0,1)$, and it is used to determine the transition event that occurs. If $0 < r_2 < a_1(\mathbf{x})/a_0$, then the first transition occurs; if $a_1(\mathbf{x})/a_0 < r_2 < (a_1(\mathbf{x}) + a_2(\mathbf{x}))/a_0$, then the second transition occurs, and so on. Lastly, both the time step and the number of individuals in each compartment are updated, and the process is iterated until the disease goes extinct or until the simulation time has been exceeded.

Appendix B. Numerical Methods for Optimal Path Computations.

Although the two-point boundary value problem given by (43) and (44) in Sec. (2.3) naturally suggests a shooting method for numerical solution, an alternative approach used in the present work is to combine the state and costate equations into a single second-order differential equation,

$$\begin{aligned}\ddot{x}_i = {} & \frac{\partial f_i}{\partial x_j}\dot{x}_j + (\dot{x}_l - f_l)(a^{-1})_{lj}\frac{\partial a_{ij}}{\partial x_k}\dot{x}_k - a_{ij}\frac{\partial f_k}{\partial x_j}(a^{-1})_{kl}(\dot{x}_l - f_l) \\ & + \frac{1}{2}a_{ij}(\dot{x}_k - f_k)\frac{\partial (a^{-1})_{kl}}{\partial x_j}(\dot{x}_l - f_l), \quad i = 1, \ldots, d,\end{aligned} \tag{124}$$

where $a := \sigma\sigma^T$ and we have used the summation convention over doubled indices. The supplementary boundary conditions for λ are re-expressed as Robin conditions for x at $t = t_{\mathrm{f}}$. Introduction of an artificial time T allows a simple initial condition for $x(t, T)$, generally a linear interpolant, to relax to the optimal path through

$$\begin{aligned}\frac{\partial x_i}{\partial T} = {} & \frac{\partial^2 x_i}{\partial t^2} - \frac{\partial f_i}{\partial x_j}\frac{\partial x_j}{\partial t} - \left(\frac{\partial x_l}{\partial t} - f_l\right)(a^{-1})_{lj}\frac{\partial a_{ij}}{\partial x_k}\frac{\partial x_k}{\partial t} + a_{ij}\frac{\partial f_k}{\partial x_j}(a^{-1})_{kl}\left(\frac{\partial x_l}{\partial t} - f_l\right) \\ & - \frac{1}{2}a_{ij}\left(\frac{\partial x_k}{\partial t} - f_k\right)\frac{\partial (a^{-1})_{kl}}{\partial x_j}\left(\frac{\partial x_l}{\partial t} - f_l\right).\end{aligned} \tag{125}$$

In the present work, this PDE was solved using central differences in space and a semi-implicit method in time, with the second derivative handled implicitly and the remaining terms on the right-hand side of (125) handled explicitly. The PDE was evolved in artificial time T until the maximum of the residual dropped below threshold.

The relaxation described in 125 occurs over curves parameterized by true time t. This parameterization is not convenient in cases where the true time of travel over the trajectory is infinite, such as for quasi-potential or mean exit time computations, or where the speed is highly nonuniform and the action is therefore concentrated in a particular segment of the path. It is convenient in such cases to re-parameterize the curve in terms of arclength. Following Ref. [49], we see that the action

$$\mathcal{S}_{t_{\mathrm{f}}} = \frac{1}{2}\int_{t_0}^{t_{\mathrm{f}}} \|\dot{x} - f(x)\|^2 \, dt \tag{126}$$

$$= \frac{1}{2}\int_{t_0}^{t_{\mathrm{f}}} \left((\|\dot{x}\| - \|f\|)^2 + 2\|\dot{x}\|\|f\| - 2(\dot{x}, f)\right) dt \tag{127}$$

$$\geq \int_{t_0}^{t_{\mathrm{f}}} (\|\dot{x}\|\|f\| - (\dot{x}, f)) \, dt \tag{128}$$

$$= 2\int_{t_0}^{t_{\mathrm{f}}} \|\dot{x}\|\|f\| \sin^2 \frac{1}{2}\theta(t) \, dt \tag{129}$$

where θ is the angle between $\dot{x}$ and $f(x)$. In the case of infinite-time paths, time can be rescaled to force

$$\|\dot{x}\| = \|f(x)\|, \tag{130}$$

so that the above inequality becomes an equality, and

$$V(0, y) = 2 \inf_{\gamma} \int_{\gamma} \|f(x(\alpha))\| \sin^2 \frac{1}{2}\theta(\alpha) \, d\alpha, \tag{131}$$

i.e., the time-parameterized minimization can be replaced by a minimization using arclength as a parameter, where in (131) the admissible paths are absolutely continuous. This approach to the numerical computation of Wentzell-Freidlin action minimizers is referred to as the geometric minimum-action method (GMAM), and requires a modification of 125 to simultaneously compute the time parameterization. The reader is referred to Ref. [49] for more details.

A similar method that employs a direct, fully explicit iterative scheme is the iterative action minimization method (IAMM) [61]. The IAMM is useful in the general situation where a path connecting steady states C_a and C_b starts at C_a at $t = -\infty$ and ends at C_b at $t = +\infty$. A time parameter t exists such that $-\infty < t < \infty$. For this method, we require a numerical approximation of the time needed to leave the region of C_a and arrive in the region of C_b. Therefore, we define a time T_ϵ such that $-\infty < -T_\epsilon < t < T_\epsilon < \infty$. Additionally, $C(-T_\epsilon) \approx C_a$ and $C(T_\epsilon) \approx C_b$. In other words, the solution stays very near the equilibrium C_a for $-\infty < t \leq -T_\epsilon$, has a transition region from $-T_\epsilon < t < T_\epsilon$, and then stays near C_b for $T_\epsilon < t < +\infty$. The interval $[-T_\epsilon, T_\epsilon]$ is discretized into n segments using a uniform step size $h = (2T_\epsilon)/n$ or a suitable non-uniform step size h_k. The corresponding time series is $t_{k+1} = t_k + h_k$.

The derivative of the function value $\mathbf{q}_k$ is approximated using central finite differences by the operator δ_h given as

$$\frac{d}{dt}\mathbf{q}_k \approx \delta_h \mathbf{q}_k \equiv \frac{h_{k-1}^2 \mathbf{q}_{k+1} + (h_k^2 - h_{k-1}^2)\mathbf{q}_k - h_k^2 \mathbf{q}_{k-1}}{h_{k-1} h_k^2 + h_k h_{k-1}^2}, \quad k = 0, \ldots, n. \tag{132}$$

Clearly, if a uniform step size is chosen then Eq. (132) simplifies to the familiar form given as

$$\frac{d}{dt}\mathbf{q}_k \approx \delta_h \mathbf{q}_k \equiv \frac{\mathbf{q}_{k+1} - \mathbf{q}_{k-1}}{2h}, \quad k = 0, \ldots, n. \tag{133}$$

Thus, one can develop the system of nonlinear algebraic equations

$$\delta_h \mathbf{x}_k - \frac{\partial H(\mathbf{x}_k, \mathbf{p}_k)}{\partial \mathbf{p}} = 0, \quad \delta_h \mathbf{p}_k + \frac{\partial H(\mathbf{x}_k, \mathbf{p}_k)}{\partial \mathbf{x}} = 0, \quad k = 0, \ldots, n, \tag{134}$$

which is solved using a general Newton's method. We let

$$\mathbf{q}_j(\mathbf{x}, \mathbf{p}) = \{\mathbf{x}_{1,j} \ldots \mathbf{x}_{n,j}, \mathbf{p}_{1,j} \ldots \mathbf{p}_{n,j}\}^T \tag{135}$$

be an extended vector of $2nN$ components that contains the j^{th} Newton iterate, where N is the number of populations. When $j = 0$, $\mathbf{q}_0(\mathbf{x}, \mathbf{p})$ provides the initial "guess" as to the location of the path that connects C_a and C_b. Given the j^{th} Newton iterate $\mathbf{q}_j$, the new $\mathbf{q}_{j+1}$ iterate is found by solving the linear system

$$\mathbf{q}_{j+1} = \mathbf{q}_j - \frac{\mathbf{F}(\mathbf{q}_j)}{\mathbf{J}(\mathbf{q}_j)}, \tag{136}$$

where $\mathbf{F}$ is the function defined by Eq. (134) acting on $\mathbf{q}_j$, and $\mathbf{J}$ is the Jacobian. Equation (136) is solved using LU decomposition with partial pivoting.

Acknowledgments. We warmly thank Lora Billings for her insight and Michael Khasin for reading and commenting on an early version of the manuscript. We also gratefully acknowledge support from the National Science Foundation awards CMMI-1233397 (EF), DMS-1418956 (EF), and DMS-1109278 (ROM).

REFERENCES

[1] D. A. Adams, L. M. Sander, and R. M. Ziff, *The barrier method: A technique for calculating very long transition times*, The Journal of Chemical Physics, 133 (2010), p. 124103.

[2] W. C. Allee, *Animal Aggregations, a Study in General Sociology*, Univ. Chicago Press, 1931.

[3] D. Anderson, M. Lisak, and A. Berntson, *A variational approach to nonlinear evolution equations in optics*, Pramana, 57 (2001), pp. 917–936.

[4] H. Andersson and B. Djehiche, *A threshold limit theorem for the stochastic logistic epidemic*, J. App.. Prob., 35 (1998), pp. 662–670.

[5] M. Assaf and B. Meerson, *Spectral theory of metastability and extinction in a branching-annihilation reaction*, Phys. Rev. E, 75 (2007), p. 031122.

[6] ———, *Extinction of metastable stochastic populations*, Phys. Rev. E, 81 (2010), p. 021116.

[7] M. Assaf, E. Roberts, and Z. Luthey-Schulten, *Determining the stability of genetic switches: Explicitly accounting for mRNA noise*, Phys. Rev. Lett., 106 (2011), p. 248102.

[8] B. G. Bale and J. N. Kutz, *Variational method for mode-locked lasers*, Journal of the Optical Society of America B, 25 (2008), p. 1193.

[9] C. Bao, A. C. Funk, C. Yang, and S. T. Cundiff, *Pulse dynamics in a mode-locked fiber laser and its quantum limited comb frequency uncertainty*, Optics Letters, 39 (2014), p. 3266.

[10] M. Bauver, E. Forgoston, and L. Billings, *Computing the optimal path in stochastic dynamical systems*, Chaos, 26 (2016), p. 083101.

[11] L. Billings and E. Forgoston, *Seasonal forcing in stochastic epidemiology models*, Ricerche di Matematica, accepted (2017).

[12] B. Z. Bobrovsky and Z. Schuss, *A Singular Perturbation Method for the Computation of the Mean First Passage Time in a Nonlinear Filter*, SIAM Journal on Applied Mathematics, 42 (1982), pp. 174–187.

[13] A. E. Bryson and Y.-C. Ho, *Applied optimal control: optimization, estimation, and control*, Taylor & Francis, Levittown, PA, 2001.

[14] D. S. Cargill and R. O. Moore, *Incorporating Radiation in Noise-Induced Phase Evolution of Optical Solitons*, SIAM Journal on Applied Dynamical Systems, 15 (2016), pp. 1025–1061.

[15] D. S. Cargill, R. O. Moore, and C. J. McKinstrie, *Noise bandwidth dependence of soliton phase in simulations of stochastic nonlinear Schrdinger equations*, Opt. Lett., 36 (2011), pp. 1659–1661.

[16] A. Chernykh and M. Stepanov, *Large negative velocity gradients in burgers turbulence*, Physical Review E, 64 (2001), p. 026306.

[17] W. Cousins and T. P. Sapsis, *Reduced-order precursors of rare events in unidirectional nonlinear water waves*, Journal of Fluid Mechanics, 790 (2016), pp. 368–388.

[18] G. Da Prato and J. Zabczyk, *Stochastic equations in infinite dimensions*, no. 45 in Encyclopedia of mathematics and its applications, Cambridge Univ. Press, Cambridge, digitally printed version (with corrections) ed., 2008. OCLC: 612518037.

[19] A. de Bouard and A. Debussche, *The Stochastic Nonlinear Schrodinger Equation in H1*, Stochastic Analysis & Applications, 21 (2003), p. 97.

[20] E. Desurvire, *Erbium-doped fiber amplifiers: principles and applications*, Wiley-Interscience, Hoboken, N.J, 2002.

[21] C. R. Doering, K. V. Sargsyan, and L. M. Sander, *Extinction times for birth-death processes: Exact results, continuum asymptotics, and the failure of the Fokker-Planck approximation*, Multiscale Model. Simul., 3 (2005), pp. 283–299.

[22] G. M. Donovan and W. L. Kath, *Rare event simulation of the performance of an actively mode-locked fiber laser model*, in Photonic Applications Systems Technologies Conference, 2007.

[23] J. L. Doob, *Topics in the theory of markoff chains*, Transactions of the American Mathematical Society, 52 (1942), pp. 37–64.

[24] M. I. Dykman and M. A. Krivoglaz, *Theory of fluctuational transitions between stable states of a nonlinear oscillator*, Sov. Phys. JETP, 50 (1979), pp. 30–37.

[25] M. I. Dykman, E. Mori, J. Ross, and P. M. Hunt, *Large fluctuations and optimal paths in chemical-kinetics*, J. Chem. Phys., 100 (1994), pp. 5735–5750.

[26] M. I. Dykman, I. B. Schwartz, and A. S. Landsman, *Disease extinction in the presence of random vaccination*, Phys. Rev. Lett., 101 (2008), p. 078101.

[27] W. E, W. Ren, and E. Vanden-Eijnden, *Simplified and improved string method for computing the minimum energy paths in barrier-crossing events*, The Journal of Chemical Physics, 126 (2007), p. 164103.

[28] V. Elgart and A. Kamenev, *Rare event statistics in reaction-diffusion systems*, Phys. Rev. E, 70 (2004), p. 041106.

[29] G. E. Falkovich, I. Kolokolov, V. Lebedev, and S. K. Turitsyn, *Statistics of soliton-*

bearing systems with additive noise, Physical Review E, 63 (2001).

[30] M. Farazmand and T. P. Sapsis, *A variational approach to probing extreme events in turbulent dynamical systems*, Science Advances, 3.9 (2017), p. e1701533.

[31] R. P. Feynman and A. R. Hibbs, *Quantum Mechanics and Path Integrals*, McGraw-Hill, Inc., 1965.

[32] E. Forgoston, S. Bianco, L. B. Shaw, and I. B. Schwartz, *Maximal sensitive dependence and the optimal path to epidemic extinction*, B. Math. Biol., 73 (2011), pp. 495–514.

[33] E. Forgoston, L. Billings, P. Yecko, and I. B. Schwartz, *Set-based corral control in stochastic dynamical systems: Making almost invariant sets more invariant*, Chaos, 21 (2011), p. 013116.

[34] E. Forgoston and I. B. Schwartz, *Escape rates in a stochastic environment with multiple scales*, SIAM J. Appl. Dyn. Syst., 8 (2009), pp. 1190–1217.

[35] M. I. Freidlin and A. D. Wentzell, *On small random perturbations of dynamical system*, Russian Math. Surveys, 25 (1970), pp. 1–55.

[36] ———, *Random Perturbations of Dynamical Systems*, Springer-Verlag, 1984.

[37] T. A. Fulton and L. N. Dunkelberger, *Lifetime of the zero-voltage state in Josephson tunnel junctions*, Phys. Rev. B, 9 (1974), p. 4760.

[38] H. Gang, *Stationary solution of master equations in the large-system-size limit*, Phys. Rev. A, 36 (1987), pp. 5782–5790.

[39] C. W. Gardiner, *Handbook of Stochastic Methods for Physics, Chemistry and the Natural Sciences*, Springer-Verlag, 2004.

[40] E. Gautier, *Large deviations and support results for nonlinear Schrodinger equations with additive noise and applications*, ESAIM: Probability and Statistics, 9 (2005), pp. 74–97.

[41] E. Gautier, *Uniform large deviations for the nonlinear Schrodinger equation with multiplicative noise*, Stochastic processes and their applications, 115 (2005), pp. 1904–1927.

[42] B. Gaveau, M. Moreau, and J. Toth, *Decay of the metastable state in a chemical system: Different predictions between discrete and continuous models*, Lett. Math. Phys., 37 (1996), pp. 285–292.

[43] D. T. Gillespie, *Exact stochastic simulation of coupled chemical reactions*, The Journal of Physical Chemistry, 81 (1977), pp. 2340–2361.

[44] P. Hänggi, P. Talkner, and M. Borkovec, *Reaction-rate theory: fifty years after kramers*, Reviews of modern physics, 62 (1990), p. 251.

[45] M. Hairer and H. Shen, *A central limit theorem for the KPZ equation*, The Annals of Probability, 45 (2017), pp. 4167–4221.

[46] M. Hairer and H. Weber, *Large deviations for white-noise driven, nonlinear stochastic PDEs in two and three dimensions*, Annales de la Faculte des Sciences de Toulouse Mathematiques, 24 (2015), pp. 55–92.

[47] C. Hartmann and C. Schtte, *Efficient rare event simulation by optimal nonequilibrium forcing*, Journal of Statistical Mechanics: Theory and Experiment, 2012 (2012), p. P11004.

[48] C. R. Heckman, M. A. Hsieh, and I. B. Schwartz, *Going with the flow: enhancing switching rates in multi-gyre systems. accepted to the asme journal of dynamic systems*, Measurement and Control, (2014).

[49] M. Heymann and E. Vanden-Eijnden, *The geometric minimum action method: A least action principle on the space of curves*, Communications on Pure and Applied Mathematics, 61 (2008), pp. 1052–1117.

[50] E. Iannone, F. Matera, A. Mecozzi, and M. Settembre, *Nonlinear Optical Communications Networks*, John Wiley & Sons, Inc., New York, 1998.

[51] D. J. Jones, S. A. Diddams, J. K. Ranka, A. Stentz, R. S. Windeler, J. L. Hall, and S. T. Cundiff, *Carrier-envelope phase control of femtosecond mode-locked lasers and direct optical frequency synthesis*, Science, 288 (2000), pp. 635–639.

[52] H. Jónsson, G. Mills, and K. W. Jacobsen, *Nudged elastic band method for finding minimum energy paths of transitions*, 1998.

[53] D. G. Kendall, *An artificial realization of a simple" birth-and-death" process*, Journal of the Royal Statistical Society. Series B (Methodological), 12 (1950), pp. 116–119.

[54] D. A. Kessler and N. M. Shnerb, *Extinction rates for fluctuation-induced metastabilities: A real space WKB approach*, J. Stat. Phys., 127 (2007), pp. 861–886.

[55] E. Khain, M. Khasin, and L. M. Sander, *Spontaneous formation of large clusters in a lattice gas above the critical point*, Phys. Rev. E, 90 (2014), p. 062702.

[56] Y. S. Kivshar and B. A. Malomed, *Dynamics of solitons in nearly integrable systems*, Rev. Mod. Phys., 61 (1989), pp. 763–915.

[57] R. V. Kohn, M. G. Reznikoff, and E. Vanden-Eijnden, *Magnetic elements at finite temperature and large deviation theory*, J. Nonlinear Sci., 15 (2005), pp. 223–253.

[58] H. A. Kramers, *Brownian motion in a field of force and the diffusion model of chemical reactions*, Physica, 7 (1940), pp. 284–304.

[59] R. J. Kryscio and C. Lefévre, *On the extinction of the s-i-s stochastic logistic epidemic*, J. App. Prob., 26 (1989), pp. 685–694.

[60] R. Kubo, K. Matsuo, and K. Kitahara, *Fluctuation and relaxation of macrovariables*, J. Stat. Phys., 9 (1973), pp. 51–96.

[61] B. S. Lindley and I. B. Schwartz, *An iterative action minimizing method for computing optimal paths in stochastic dynamical systems*, Physica D, 255 (2013), pp. 22–30.

[62] D. G. Luchinsky, P. V. E. McClintock, and M. I. Dykman, *Analogue studies of nonlinear systems*, Rep. Prog. Phys., 61 (1998), pp. 889–997.

[63] B. J. Matkowsky and Z. Schuss, *The exit problem for randomly perturbed dynamical systems*, SIAM Journal on Applied Mathematics, 33 (1977), pp. 365–382.

[64] M. A. Mohamad, W. Cousins, and T. P. Sapsis, *A probabilistic decomposition-synthesis method for the quantification of rare events due to internal instabilities*, Journal of Computational Physics, 322 (2016), pp. 288–308.

[65] M. A. Mohamad and T. P. Sapsis, *Probabilistic response and rare events in Mathieu's equation under correlated parametric excitation*, Ocean Engineering, 120 (2016), pp. 289–297.

[66] R. O. Moore, *Trade-off between linewidth and slip rate in a mode-locked laser model*, Optics Letters, 39 (2014), p. 3042.

[67] R. O. Moore, G. Biondini, and W. L. Kath, *A Method to Compute Statistics of Large, Noise-Induced Perturbations of Nonlinear Schroedinger Solitons*, SIAM Review, 50 (2008), p. 523.

[68] R. O. Moore, T. Schaefer, and C. K. Jones, *Soliton broadening under random dispersion fluctuations: Importance sampling based on low-dimensional reductions*, Optics Communications, 256 (2005), pp. 439–450.

[69] I. Nåsell, *The quasi-stationary distribution of the closed endemic sis model*, Advances App. Prob., 28 (1996), pp. 895–932.

[70] ———, *On the time to extinction in recurrent epidemics*, J. R. Statist. Soc. B, 61 (1999), pp. 309–330.

[71] G. Nieddu, L. Billings, and E. Forgoston, *Analysis and control of pre-extinction dynamics in stochastic populations*, B. Math. Biol., 76 (2014), pp. 3122–3137.

[72] G. T. Nieddu, L. Billings, J. H. Kaufman, E. Forgoston, and S. Bianco, *Extinction pathways and outbreak vulnerability in a stochastic ebola model*, Journal of The Royal Society Interface, 14 (2017), p. 20160847.

[73] B. Øksendal, *Stochastic differential equations: an introduction with applications*, Universitext, Springer, Berlin, 6. ed., 6. corrected printing ed., 2013. OCLC: 935584333.

[74] O. Ovaskainen and B. Meerson, *Stochastic models of population extinction*, Trends in Ecol. and Evol., 25 (2010), pp. 643–652.

[75] R. Paschotta, A. Schlatter, S. Zeller, H. Telle, and U. Keller, *Optical phase noise and carrier-envelope offset noise of mode-locked lasers*, Applied Physics B, 82 (2005), pp. 265–273.

[76] G. A. Pavliotis, *Stochastic processes and applications*, Springer, 2011.

[77] H. Risken, *The Fokker-Planck Equation*, Springer-Verlag, 1996.

[78] E. Roberts, S. Be'er, C. Bohrer, R. Sharma, and M. Assaf, *Dynamics of simple gene-network motifs subject to extrinsic fluctuations*, Phys. Rev. E, 92 (2015), p. 062717.

[79] I. B. Schwartz, L. Billings, M. Dykman, and A. Landsman, *Predicting extinction rates in stochastic epidemic models*, J. Stat. Mech.-Theory E., (2009), p. P01005.

[80] I. B. Schwartz, E. Forgoston, S. Bianco, and L. B. Shaw, *Converging towards the optimal path to extinction*, J. R. Soc. Interface, 8 (2011), pp. 1699–1707.

[81] M. Shtaif and C. Menyuk, *Carrier envelope phase locked modelocking in fiber lasers at ultra-high repetition rates*, in CLEO: Science and Innovations, Optical Society of America, 2011, p. CMD6.

[82] R. C. Smith, *Uncertainty quantification: theory, implementation, and applications*, Computational science and engineering series, Society for Industrial and Applied Mathematics, Philadelphia, 2013.

[83] E. T. Spiller, W. L. Kath, R. O. Moore, and C. J. McKinstrie, *Computing large signal distortions and bit-error ratios in DPSK transmission systems*, IEEE Photonics Technology Letters, 17 (2005), pp. 1022 –1024.

[84] H. Touchette, *The large deviation approach to statistical mechanics*, Physics Reports, 478 (2009), pp. 1–69.

[85] L. S. Tsimring, *Noise in biology*, Reports on Progress in Physics, 77 (2014), p. 026601.

[86] N. G. van Kampen, *Stochastic Processes in Physics and Chemistry*, Elsevier, 2007.

[87] E. Vanden-Eijnden and J. Weare, *Data assimilation in the low noise, accurate observation regime with application to the Kuroshio current*, arXiv:1202.4952, (2012).

[88] ———, *Rare event simulation of small noise diffusions*, Communications on Pure and Applied Mathematics, 65 (2012), pp. 1770–1803.

[89] J. Ye, H. Schnatz, and L. Hollberg, *Optical frequency combs: From frequency metrology to optical phase control*, IEEE Journal of Selected Topics in Quantum Electronics, 9 (2003), pp. 1041–1058.

[90] W. Zhang, H. Wang, C. Hartmann, M. Weber, and C. Schuette, *Applications of the cross-entropy method to importance sampling and optimal control of diffusions*, SIAM Journal on Scientific Computing, 36 (2014), pp. A2654–A2672.